NASA TN D-1214


# TECHNICAL NOTE

## D-1214

# INVESTIGATION OF FORCED-CONVECTION NUCLEATE BOILING OF WATER FOR NOZZLE COOLING AT VERY HIGH HEAT FLUXES

By John W. Schaefer and John R. Jack

Lewis Research Center
Cleveland, Ohio

NATIONAL AERONAUTICS AND SPACE ADMINISTRATION
WASHINGTON
May 1962

NATIONAL AERONAUTICS AND SPACE ADMINISTRATION

TECHNICAL NOTE D-1214

# INVESTIGATION OF FORCED-CONVECTION NUCLEATE BOILING OF WATER FOR NOZZLE COOLING AT VERY HIGH HEAT FLUXES

By John W. Schaefer and John R. Jack

## SUMMARY

Forced-convection nucleate boiling of water in axial flow was investigated experimentally as a means of cooling the nozzle of an electrothermal engine, electric-arc wind tunnel, or nuclear rocket. The nonuniform axial heat-flux distribution typical of a very high temperature flow nozzle was simulated by resistance heating of variable-wall-thickness Inconel tubes. The coolant water flowed through the constant-inside-diameter test sections at flow rates ranging from $0.45 \times 10^4$ to $1.27 \times 10^4$ lb/(sq ft)(sec) (inlet velocities of 73 to 204 ft/sec). Steady-state nucleate boiling was maintained at local heat fluxes as high as 11,200 Btu/(sq ft)(sec) ($40.3 \times 10^6$ Btu/(sq ft)(hr)). Nucleate-boiling heat-transfer results were obtained for the complete range of flow rates at pressures from 69 to 296 pounds per square inch absolute and were compared with existing correlations. The nonboiling forced-convection heat-transfer results were correlated by the Colburn equation with a modified coefficient. The burnout heat flux in the high range of flow rates was determined and is compared with existing prediction techniques. The pressure drop both with and without heat addition was also investigated.

The solution for the temperature distribution in a resistance-heated variable-wall-thickness tube is presented in an appendix. The appropriate heat-transfer and electrical relations are also presented.

## INTRODUCTION

The very high heat fluxes encountered in the vicinity of the nozzle throat of an electrothermal engine, electric-arc wind tunnel, or nuclear rocket present a severe cooling problem. Local heat fluxes of the order of 10,000 Btu/(sq ft)(sec) are not improbable in a high-performance unit. This may be compared with a typical value of 600 Btu/(sq ft)(sec) for a chemical rocket (ref. 1). In fact, it has been suggested in reference 2

that the high-enthalpy, high-pressure operation of plasma generators may ultimately be limited by heat-transfer problems. The general feasibility study of cooling electrothermal thrust generators presented in reference 3 shows that the performance of these propulsion devices is indeed limited by the attendant cooling problems. Therefore, improvement of the performance capabilities of these high-temperature devices is dependent on the development of better cooling techniques. One attractive method of improving cooling capabilities is to take advantage of the high heat-transfer coefficients associated with forced-convection nucleate boiling.



The axial heat-flux distribution in a nozzle is nonuniform with a severe gradient and peak heating occurring in the vicinity of the nozzle throat. Nucleate-boiling results at these very high heat fluxes are not available. However, at low heat flux and low flow rate, a number of investigations have been performed (e.g., refs. 4 to 6) and are summarized by McAdams (ref. 7). Because of the paucity of data, the generally accepted correlation equations such as those in references 4 and 8 have not been shown to be applicable at the severe conditions associated with nozzles having very high heat fluxes.

The upper limit for successful cooling by forced-convection nucleate boiling is obtained when the burnout heat flux is reached; that is, the flux at which transition to film boiling occurs. Several correlations have been developed for prediction of burnout in a forced-convection axial-flow system with a uniform heat flux distribution (e.g., ref. 9). These correlations indicate that successful cooling of extremely high heat fluxes requires flow rates that result in prohibitive pressure drops. High burnout heat fluxes have been attained only with vortex or swirl flow (refs. 10 and 11). Again, however, the pressure drop is large.

Techniques for prediction of the burnout heat flux and burnout location for a nonuniform heat-flux distribution such as that found in a nuclear-reactor fuel element have been presented by Bernath (ref. 12) and Sonnemann (ref. 13). Both procedures require the use of a uniform heat-flux correlation. Sonnemann applied his technique to some experimental results for a chopped cosine - axial heat-flux distribution and found good agreement. However, the applicability of these techniques to a distribution typical of a high-temperature-flow nozzle appears highly questionable in the light of the large heat-flux gradient and the high maximum flux.

It is apparent, therefore, that nucleate-boiling results are not available for the conditions anticipated in a very high temperature flow nozzle and that available approaches for predicting the upper limit of nucleate boiling (burnout) appear inadequate. This investigation was initiated to determine the possibilities of and requirements for cooling the high nozzle heat fluxes associated with high-temperature flows by

forced-convection nucleate boiling of water with simple axial flow. In addition, the applicability of available correlations and prediction techniques at these high fluxes was investigated. The nozzle flux distribution was simulated by resistance heating of various Inconel tubes with an axial variation in wall thickness. Nucleate-boiling and nonboiling forced-convection heat-transfer and pressure-drop results are presented for axial flow of water at heat fluxes up to 11,200 Btu/(sq ft)(sec) and flow rates from $0.45\times10^4$ to $1.27\times10^4$ lb/(sq ft)(sec) (inlet velocities from 73 to 204 ft/sec). Burnout heat flux results in the high range of flow rates are also presented.

## APPARATUS AND PROCEDURE

### Flow System

A schematic diagram of the flow system is shown in figure 1. Distilled water flowed downward through the vertically mounted test sections. (Because of the high flow rates, the effect of free convection is negligible.) The distilled water was circulated in a closed loop by a variable-speed-drive positive-displacement pump with a maximum outlet pressure of 800 pounds per square inch gage. Power was supplied to the test sections by a direct-current generator with a continuously variable voltage from 0 to 500 volts (maximum current of 6000 amp). In all tests a ballast resistor of at least three times the test-section resistance was in series with the test section to allow a fine control of the current.

The possibility of flow instability and scale formation was eliminated as much as practicable by proper flow system design and test procedures (see ref. 9). The main throttle, upstream of the test section, was required to maintain a large pressure drop that acted as a bucking pressure to prevent flow fluctuations inherent in boiling and the resultant premature burnout. The pressure drop across the main throttle and test section to the point at which burnout would occur was 200 pounds per square inch or higher for all tests.

To reduce the possibility of flow fluctuations due to compressible volumes, the Bourdon tube of the test-section inlet pressure gage was filled with water, and the line to the gage was purged before each test. To inhibit rust formation and the resultant test-section scale problem the reservoir and all water lines except for small lengths of high-pressure hose were stainless steel. The pump case, however, was steel. Therefore, to eliminate as much oxygen from the system as practicable, a nitrogen atmosphere was maintained in the reservoir, and the reservoir was pressurized so as to maintain all points in the flow system above atmospheric pressure. The reservoir was evacuated to approximately

15 inches of mercury vacuum and repressurized with nitrogen at least once before a series of tests; the reservoir pressure ranged from 2 to 20 pounds per square inch gage. Since the amount of dissolved gas due to the nitrogen atmosphere in the reservoir was small and since all tests were run with highly subcooled water (bulk temperature well below the saturation temperature), it is felt that dissolved gas had a negligible effect on the nonboiling and burnout results and at most a small effect on the nucleate-boiling results.

The results for all tests were obtained with clean untreated distilled water. After each series of tests the reservoir was emptied and refilled with a new charge of water to prevent the possibility of scale formation. Results were continually checked for the effect of scale formation throughout each test series. All results presented are for tests with negligible scale.



## Test Sections

The nominal geometries of the test sections are shown in figure 2. The test sections were fabricated from commercially available constant-wall-thickness Inconel tubing by machining the outside diameter. Inconel was chosen as the test-section material mainly because of its low thermal coefficient and high value of electrical resistivity. Over the heated length, the wall thickness decreased linearly from either end to a minimum at the center. The test-section inside diameter was measured with a set of pin gages, and the outside diameter $(d_o)_1$ (see fig. 2) was measured with a comparator at 100 power. (Symbols are defined in appendix A.) The minimum wall thickness $t_1$ determined from these two measurements was felt to be within ±0.005 inch. The concentricity of the outside and inside diameters was checked by observation of the local circumferential uniformity in test-section color at high wall temperature. The validity of this technique was verified by measurements on two test sections that were cut in half after test. Results were obtained only for test sections with a uniform circumferential wall thickness and, therefore, uniform circumferential heat flux. The absence of a forming effect during machining was also verified from the two cut test sections. The dimensions $l$ and $(d_o)_o$ (see fig. 2) were measured with the comparator at 20 power.

The calculated nominal flux distribution for all test sections, assuming all heat enters the stream and neglecting axial conduction (which, for the conditions of this investigation, is valid), is shown in figure 2. The variation in heat flux at the minimum-wall-thickness point was made continuous by machining a small radius of transition between the linear tapers. The throat section of a preliminary nozzle design for the Lewis Research Center arc tunnel and the associated heat-flux distribution based on a theoretical isothermal-boundary-layer calculation (ref. 14) for air is shown in figure 3. For comparison the test-section heat-flux distribution (fig. 2) for $l = 2.75$ inches and

$q$ equal the maximum heat flux of figure 3 is also presented. The experimental flux distribution of this investigation is representative of a nozzle with a radius of curvature at the throat smaller than that of figure 3. It should be noted that the cooling channels for an actual nozzle (fig. 3) are sections of an annulus with one-side heating, whereas the test configuration is circular with uniform circumferential heating. The results presented are therefore indicative of but not necessarily quantitatively applicable to an actual nozzle configuration.



A closeup view of a test section installed in the test rig is shown in figure 4. Small copper disks were silver-soldered to the test section at appropriate distances from each end for fastening to the larger copper buss heads. An O-ring provided the water seal between the disk and the buss head. Large stainless-steel split washers were used to ensure good electrical contact between the disk and head.

## Instrumentation

Outside test-section wall temperatures were measured with Chromel-Alumel thermocouples spotwelded directly to the wall. Since a direct current passed through the test sections, any displacement of the effective contact point of one thermocouple lead from the other resulted in a small voltage drop between the two leads in addition to the thermocouple output. To account for this direct-current component, tests were run at identical conditions with opposite directions of current flow. The average of the two thermocouple readings yielded the thermocouple output due to temperature only. The inlet and outlet bulk temperatures of the circulating water were measured with copper-constantan thermocouples in mixing chambers immediately upstream and downstream of the test section. The water flow rate was determined from a turbine-type flowmeter.

Current was determined by measuring the voltage drop across a calibrated shunt connected in series with the test section. The voltage drop across the test section was read from a direct-current voltmeter connected between the two copper buss heads.

The inlet and outlet static pressures were read on high-accuracy pressure gages. The static-pressure taps were located in short transition sections upstream and downstream of the test section. The inside diameter matched that of the test sections.

## DATA REDUCTION

Evaluation of the test data required a knowledge of the thermal conductivity and electrical resistivity of Inconel and their variation with temperature. The thermal conductivity was obtained from reference 15 and is presented in figure 5. The agreement with average values over

a number of temperature ranges published in reference 16 was good. A linear equation of the form $k = k_r(1 + \alpha T)$ was used for data reduction (see appendix B); the line used is also presented in the figure. The electrical resistivity and its variation with temperature were obtained from tests on samples of tubing used for test-section fabrication. Consistent results were obtained and are presented in figure 5. The room-temperature value agrees favorably with published results. Since the temperature variation of electrical resistivity was small (a maximum increase of about 5 percent over the room-temperature value), the equations developed for reduction of data (appendixes B and C) assume constant resistivity.



The coolant-side wall temperature at any axial location was determined from equation (B14):

$$u(\eta, \theta_o) = u_o - C_o \frac{I^2\sigma}{2k_r b^2} - \frac{\eta\theta_o^2}{2}\left[\eta\left(\frac{\partial^2 u}{\partial \eta^2}\right)_o + \left(\frac{\partial u}{\partial \eta}\right)_o\right] \tag{B14a}$$

where

$$b^2 = \frac{2\left[\pi\eta\theta_o(\eta\theta_o + d_i)\right]^2}{r_o^2\left[\left(\frac{r_i}{r_o}\right)^2 + 2\ln\frac{r_o}{r_i} - 1\right]} \tag{B21a}$$

The geometry variables are defined in figure 6. The temperature parameter $u$ is given by $u = T\left(1 + \frac{\alpha}{2}T\right)$, and $\alpha$ and $k_r$ are presented in figure 5. The conduction term is zero at the minimum-wall-thickness location $y = 0$ because of the radius of transition between the tapered sections discussed previously. At all other axial locations the conduction term was found to be negligible for all tests.

The heat flux at any axial location was calculated from equation (C9):

$$q_i = C_o \frac{I^2\sigma}{\pi^2 d_i \eta\theta_o(\eta\theta_o + d_i)} - \frac{\eta\theta_o(\eta\theta_o + d_i)}{d_i} k_r\left(\frac{1}{\eta}\frac{d\bar{u}}{d\eta} + \frac{d^2\bar{u}}{d\eta^2}\right) \tag{C9}$$

where $\bar{u}$ is given by equation (C7). Again the conduction term is zero at $y = 0$ and was found to be negligible at all other locations.

In all tests sufficient data were taken to allow checks on test-section performance. The test-section resistance was determined from

equation (C2) and from the measured voltage drop across the test section. The heat input to the water was determined from equation (C4) and from the temperature rise through the test section. (The exit water was always highly subcooled, i.e., well below the saturation temperature.) In every test, agreement between the two methods of calculation was good.

The equations for data reduction require a small taper angle $\theta_o$, no temperature variation of electrical resistivity, a linear variation of thermal conductivity, and an insulated outside wall. All assumptions were reasonably satisfied: The maximum $\theta_o$ was $3\frac{1}{2}^\circ$, the temperature variation of resistivity was small, the linear conductivity relation fits the experimental results very well in the temperature range of interest, and the radiation and convection losses from the outside wall were determined to be negligible in all cases.

The bulk water temperature at the maximum-heat-flux location was taken as the average of the inlet and outlet temperatures. The bulk temperature distribution was determined from equation (C10), which becomes over the complete heated length:

$$T_b(\eta) = T_{in} + \frac{T_{out} - T_{in}}{2}\left\{1 \pm \frac{\ln\left[\left(\frac{\eta}{\eta_1}\right)\left(\frac{\eta_1\theta_o + d_i}{\eta\theta_o + d_i}\right)\right]}{\ln\left[\left(\frac{\eta_o}{\eta_1}\right)\left(\frac{\eta_1\theta_o + d_i}{\eta_o\theta_o + d_i}\right)\right]}\right\} \qquad (1)$$

where $\eta$ must be applied separately for the upstream and downstream lengths (see fig. 6), and the negative sign applies to the upstream length and the positive sign to the downstream length.

The axial static-pressure distribution was assumed to be linear. In some tests the outlet pressure was not measured. The pressure distribution was therefore determined from the available pressure-drop results.

Considering all possible sources of error, an estimate of the maximum errors in the results is as follows:

| | |
|---|---|
| $q_1$, percent | ±7 |
| q (other than at y = 0), percent | ±10 |
| $(T_w)_1$, percent | ±5 |
| $T_w$ (other than at y = 0), percent | ±10 |
| $T_{sat}$, °F | ±4 |
| $T_b$, °F | ±4 |
| $\Delta p$, percent | ±5 |

The maximum error in heat-transfer coefficient is estimated to be ±18 percent for the results at $y = 0$ and ±28 percent for results at other axial locations. The possible error is largest for a small temperature difference $T_w - T_b$.

In a number of tests an entrance effect was observed that resulted in abnormally low heat-transfer coefficients for a short distance downstream of the test-section inlet. In these tests a slight misalinement at the inlet transition section and the test section apparently caused cavitation. Tests in which the heat-transfer coefficient at $y = 0$ on a short heated length test section with both a smooth junction and a slightly misalined junction demonstrated that the observed effect was actually due to a disturbance at the test-section inlet. No heat-transfer results are presented in the region over which the entrance effect occurred.



## RESULTS AND DISCUSSION

### Heat Transfer

All heat-transfer results obtained at the maximum-heat-flux location $y = 0$ are presented in figure 7 and table I. As shown in the figure the points in order of increasing wall temperature represent nonboiling forced-convection heat transfer, forced-convection nucleate-boiling heat transfer, and burnout. The nucleate-boiling points are identified according to flow rate and saturation temperature. The burnout points indicate only heat flux; no temperature difference $T_w - T_b$ is associated with them. The maximum experimental heat flux obtained was 11,700 Btu/(sq ft)(sec); the flow rates and inlet velocities ranged from $0.45 \times 10^4$ to $1.27 \times 10^4$ lb/(sq ft)(sec) and 73 to 204 feet per second, respectively. Pressures ranged from 69 to 307 pounds per square inch absolute, and all nucleate-boiling results are at high subcooling $T_{sat} - T_b$. All results are presented in terms of local values.

Nonboiling forced convection. - The three basic turbulent pipe flow correlations (ref. 7) are those of Dittus and Boelter, Sieder and Tate, and Colburn. These equations are strictly applicable only for the case of an isothermal wall. The experimental wall temperature distribution of this investigation is nonuniform, however, because of the imposed flux distribution as shown in figure 2. Comparison of experiment with these correlations is therefore not strictly valid. As shown, for example, in reference 17, a nonisothermal wall upstream of a point may appreciably affect the heat transfer at that point. (This effect is in addition to any conduction effect.) The magnitude of this effect for the experimental wall temperature distributions was estimated by

the method of reference 17. The axial distribution of the ratio of nonisothermal heat-transfer coefficient to isothermal heat-transfer coefficient $h_{noniso}/h_{iso}$ was determined. This ratio at the maximum-heat-flux location $y = 0$ was found to be of the order of 1.10. (The three cases calculated yielded values of 1.08, 1.10, and 1.12.) This ratio times the predictions of the previously mentioned correlation equations allows comparison with the experimental results.



As shown in figure 7 the Dittus and Boelter equation, uncorrected for the nonisothermal effect, underestimates the experimental heat transfer at the maximum-heat-flux location $y = 0$. If the nonisothermal correction is included, the correlation still underestimates the experimental heat transfer at large temperature difference and also does not predict the trend of experiment. The Sieder-Tate equation, uncorrected or corrected, also underestimated the experimental heat transfer, and a large amount of scatter was apparent when the experimental results were plotted in terms of the correlation parameters.

All nonboiling experimental points at the maximum-heat-flux location $y = 0$ are presented in figure 8 in terms of the Colburn equation variables. Also included are the Colburn equation and the Colburn equation with the nonisothermal correction (at $y = 0$). The experimental points fall below both the uncorrected and corrected correlation equations; and, in fact, the correction results in poorer agreement. The form of the Colburn equation, however, in which the Reynolds and Prandtl numbers are evaluated at the film temperature $T_f = (T_w + T_b)/2$, brings the results together quite well (fig. 8). (A small increase in the exponent of the Prandtl number would yield a slightly better fit of the experimental points; however, it is felt that the small amount of data and the general validity of the form of the Colburn equation do not warrant presentation of another fit of the data.) The experimental nonboiling heat transfer at $y = 0$ (fig. 8) is therefore represented approximately by the equations

$$St = \frac{0.021}{Re_f^{0.2} Pr_f^{2/3}} \tag{2a}$$

$$h = \frac{0.021(\rho v)(c_p)_b}{Re_f^{0.2} Pr_f^{2/3}} \tag{2b}$$

where all properties except specific heat are evaluated at the film temperature $T_f$. The constant 0.021 may be contrasted with the value of approximately 0.025 for the Colburn equation with the nonisothermal wall correction.

A modified isothermal equation which, when corrected for the nonisothermal effect, will fit the experimental results of figure 8 can be determined. This equation is

$$St = \frac{0.019}{Re_f^{0.2} Pr_f^{2/3}} \tag{3a}$$

or

$$h = \frac{0.019(\rho v)(c_p)_b}{Re_f^{0.2} Pr_f^{2/3}} \tag{3b}$$

When the nonisothermal correction ($h_{noniso}/h_{iso} \approx 1.10$) is applied to equations (3), agreement with experiment is apparent. Equations (3), therefore, represent the experimental results reduced to isothermal conditions.

This discussion was limited to the results at the maximum-heat-flux location $y = 0$. The correction at other axial locations was also investigated and compared with experiment. These results are presented in a following section entitled "Axial distribution of heat-transfer coefficient."

Nucleate-boiling forced convection. - The heat-transfer results at high heat flux, approximately constant subcooling $T_{sat} - T_b$, and constant saturation temperature are plotted in figure 9 at the highest flow rate, the only flow rate for which a reasonable amount of data is available over a range of heat flux. The variation is typical of that found in other investigations (see ref. 7) at lower heat fluxes and flow rates. A heat-flux - wall temperature variation typical of nonboiling forced convection holds up to wall temperatures somewhat in excess of the saturation temperature. When the wall superheat $T_w - T_{sat}$ is sufficient to initiate nucleate boiling, further increase in heat flux results in the small variation in wall temperature typical of nucleate-boiling heat transfer. The wall superheat required to initiate nucleate boiling is approximately 65° F at these conditions. Steady-state nucleate boiling at approximately the conditions of the figure was maintained at a heat flux as high as 11,200 Btu/(sq ft)(sec) for $l = 0.75$ inch (which corresponds to the burnout flux of 11,450 Btu/(sq ft)(sec) of fig. 7).

All nucleate-boiling results over the entire flow rate range are presented in figure 10 in terms of the wall superheat correlation of Jens and Lottes (ref. 4), which was derived from results at lower heat fluxes and flow rates. The heat fluxes predicted by the general semiempirical

correlation of Forster and Greif (ref. 8) for three representative tests were calculated and are also included in figure 10. The corresponding experimental and calculated points are indicated by arrows. The Jens and Lottes equation in general underestimates the ratio $(T_w - T_{sat})/q^{1/4}$. The Forster-Greif correlation, however, is seen to predict the experimental heat flux quite well. (The experimental wall and saturation temperatures were required to evaluate the predicted heat flux.)



Both correlations indicate that the relation between heat flux and wall superheat in nucleate boiling is independent of flow rate. The scatter and limited results do not allow a definite confirmation at the high range of flow rates of this investigation. No consistent flow rate effect is apparent, however.

To illustrate the effect of water contaminants on scale formation and the associated reduction in the nucleate-boiling heat-transfer coefficient, a single test was run with distilled water visibly contaminated with rust. At the maximum-heat-flux point $y = 0$, where nucleate boiling occurred, the wall temperature $T_w$ increased $239^\circ$ F in the 30-minute run at constant test conditions. The wall temperatures were unchanged at other axial locations where no boiling occurred. After testing, the test section was cut open for inspection. A reddish-brown scale indicative of a rust deposit was localized in the area of maximum heat flux.

Axial distribution of heat-transfer coefficient. - The experimental axial distributions of wall temperature, bulk temperature, and heat flux are presented in table II for nonboiling heat transfer over the entire test-section length and nucleate boiling in the area of maximum heat flux. Only results at and downstream of the maximum-heat-flux location $y \geq 0$ are presented because of the entrance effect discussed in the section entitled "Data Reduction."

The axial heat-transfer-coefficient distribution for the case of nonboiling is presented in figure 11(a). The predicted distributions presented are those obtained by evaluating the modified Colburn equation (eq. (3b)) at local conditions and those obtained by correcting this distribution for the nonisothermal wall effect. The nonisothermal wall correction is discussed in detail in a previous section, "Nonboiling forced convection." Equation (3b) corrected for the nonisothermal wall effect shows very good agreement with experiment from $y/l = 0$ to 0.5. Farther downstream the experimental points fall somewhat below the predicted variation.

The heat-transfer coefficient distribution for local nucleate boiling is presented in figure 11(b). The distribution corresponding to the plot of figure 9 (the results of which are for $y = 0$ at approx. the same mass-flow rate, subcooling, and saturation temperature in fig. 11(b))

applied at the local axial flux is presented in figure 11(b) for the region in which the wall temperature is higher than the saturation temperature. This distribution appears to be correct in the region of local nucleate boiling. The distributions predicted by applying the modified isothermal Colburn equation (eq. (3b)) locally and by including the calculated nonisothermal wall effect are presented in the region of nonboiling. The predicted nonboiling lines cannot be expected to be valid, however, since neither the correlation equation nor the nonisothermal correction allows for an upstream region of nucleate boiling. Neither of the nonboiling predictions shows agreement with experiment. Local nucleate boiling, therefore, appears to have a definite effect on the nonboiling heat transfer downstream.



Burnout. - The burnout results are included in table I and figure 7. The burnout conditions were obtained by increasing the current and, therefore, the heat flux, in small increments until catastrophic failure due to transition to film boiling occurred. The tabulated heat fluxes are therefore the maximum local flux at the burnout location ($y = 0$) at which steady-state nucleate boiling was maintained and the flux (at $y = 0$) at which catastrophic failure occurred. The burnout flux is defined as the average of these two flux conditions. No wall temperatures were obtained for the maximum steady-state boiling conditions because of the danger to test personnel in case of failure and the requirement of two tests at the identical conditions to eliminate the direct-current component on the thermocouple output.

The axial location of burnout in the three burnout runs was at the point of maximum heat flux within the accuracy of measurement after failure. The maximum local burnout heat flux was 11,450 Btu/(sq ft)(sec) at a flow rate of $1.25 \times 10^4$ lb/(sq ft)(sec) ($v_{in}$ = 202 ft/sec) and a heated length $2l$ of 1.50 inches. The two burnout fluxes obtained at these same test conditions using two different test sections show good agreement. No indication of incipient burnout, such as flow fluctuations or audible noise, was apparent.

Although burnout results are available for only two test conditions, it is interesting to compare the results with existing burnout prediction methods. The techniques for predicting burnout with an axial flux distribution presented in references 12 and 13 were applied to the heat-flux distribution of this investigation. The two techniques are basically the same: The axial location of burnout and, therefore, the heated length to burnout is determined. The maximum flux at the burnout point is then established by substituting this heated length into a uniform heat-flux burnout correlation. The uniform flux correlation developed in reference 13, however, is not applicable at the pressures of this investigation and that of reference 12 was found to predict unreasonably low burnout fluxes. A review of the available uniform flux burnout

correlations indicated that the correlation developed in reference 9 was the most comprehensive. Therefore, the technique of references 12 and 13 was used to predict the burnout location. The local burnout heat-flux prediction was then calculated by substitution of the determined heated length together with the other conditions into the correlation equation of reference 9 (uniform flux). For high flow rates this equation is

$$q_{bo} = \frac{23(\rho v)^{0.5}}{(s/d_i)^{0.15} d_i^{0.2}} \tag{4}$$

where $s$ is the heated length to burnout and the dimensional constant requires units of Btu, feet, and seconds. The calculated burnout flux then establishes the maximum flux at the point where burnout would occur.

The location of burnout was predicted to be in the immediate vicinity of the point of maximum heat flux, the same location found experimentally. This predicted location, however, is intuitively apparent from consideration of the experimental flux distribution. The heated length to burnout $s$ equals $l$, half the total heated length. Evaluation of equation (4) with the determined $s$ at the conditions associated with the experimental burnout points yielded the following results:

| Experimental burnout flux, Btu/(sq ft)(sec) | Predicted burnout flux, Btu/(sq ft)(sec) |
|---|---|
| 8,000 | 3600 |
| 11,450 | 5000 |
| 11,100 | 5000 |

The prediction method of references 12 and 13, therefore, seriously underestimates the flux at burnout. The method has been used successfully for certain flux distributions (ref. 13) but is apparently not applicable to a distribution with large gradients.

From equation (4), the ratio of two burnout heat fluxes for which the flux distributions are uniform is

$$\frac{(q_{bo})_2}{(q_{bo})_1} = \left[\frac{(\rho v)_2}{(\rho v)_1}\right]^{0.5} \left[\frac{(s/d_i)_1}{(s/d_i)_2}\right]^{0.15} \left[\frac{(d_i)_1}{(d_i)_2}\right]^{0.2} \tag{5}$$

It is interesting to compare the experimental nonuniform flux value of $(q_{bo})_2/(q_{bo})_1$ with that obtained from this equation. Since the two higher experimental burnout flux points are almost equal and at almost identical conditions, these values will be averaged and taken as $(q_{bo})_2$. Therefore, $(q_{bo})_1$ is the lower burnout flux point, 8000 Btu/(sq ft)(sec). The heated length is taken as $l$. The experimental flux ratio is 1.40, and substitution of the appropriate conditions into equation (5) yields a predicted flux ratio of 1.41. This excellent agreement suggests that an effective heated length may be defined for use in equation (4) to allow prediction of the burnout flux for the particular distribution of this investigation. This effective length may be expressed as $s' = C's$ where $s$ is the heated length to burnout ($s = l$) and $C'$ is a constant for the particular distribution. The value of $C'$ must fall in the range $0 < C' \leq 1$, where unity corresponds to a uniform flux distribution. Evaluation from equation (4) yields $C' = 0.005$. Therefore, the burnout flux for the distribution of this investigation is given by

$$q_{bo} = \frac{23(\rho v)^{0.5}}{\left(\frac{0.005\ l}{d_i}\right)^{0.15} d_i^{0.2}} \tag{6}$$

It should be emphasized that this analysis and equation must be taken with reservations since they are based on points at only two conditions.

## Pressure Drop

The experimental pressure-drop data are presented in table III for flow with no heat transfer, flow with nonboiling heat transfer, and flow with local nucleate boiling. It should be noted that the pressure-drop data include the effect of any misalinement between the test section and the inlet and outlet transition sections (in which the static-pressure taps were located). Also, a possible entrance effect existed since the inlet static-pressure tap was only 0.60 inch downstream of the sudden contraction at the inlet of the transition section.

The experimental friction factors were determined from the equation

$$f = \frac{\Delta p}{\left[\frac{4(\rho v)}{2g}\right] v_{in} \frac{L}{d_i}} \tag{7}$$

for both isothermal and heat-transfer conditions. The experimental friction factors for no heat transfer and those for local nucleate boiling

are presented in figure 12. The accepted variation for turbulent flow in a smooth tube with no heat addition from reference 7 is included. The friction factors for no heating fall above the smooth-tube line and exhibit a dependence on test-section length. This increase in friction with decreasing L/d is indicative of misalinement and entrance effects. Since the magnitude of these effects would be approximately the same for each test section, the fraction of the pressure drop associated with these effects increases with decreasing length L and is therefore more dominant for shorter lengths.



For the case of heat transfer with no local nucleate boiling, the friction factors decreased with increasing wall temperature. This is apparent from table III (wall temperature increases with heat flux). All these results fell between the no-heat-transfer results and the local-nucleate-boiling results of figure 12. This decrease in friction factor may be explained in terms of the reduced wall viscosity associated with the wall temperature and is discussed in references 5 and 18.

The effect of local nucleate boiling (nucleate boiling in the region of maximum heat flux and nonboiling elsewhere) on the pressure drop was particularly interesting. As seen from figure 12, the friction factors fall below the results for no heat transfer, are apparently independent of heat flux, and are less sensitive to Reynolds number (based on inlet conditions). These characteristics may be explained in the light of the separate effects of nucleate boiling on pressure drop and of nonboiling heat transfer on pressure drop. As discussed previously, the pressure drop for nonboiling heat transfer is lower than that without heat transfer. Conversely, the pressure drop in a section with nucleate boiling would be higher than that for nonboiling (refs. 4 and 18). Therefore, with local nucleate boiling in the test section, the pressure drop in the axial distance over which nucleate boiling occurs is higher than would be expected for nonboiling heat transfer; whereas, in the nonboiling regions, a drop occurs which is lower than that with no heat transfer. Therefore, a possible explanation of the independence of friction factor on heat flux once nucleate boiling has been initiated is as follows: An increase in heat flux causes an increase in the extent of the nucleate-boiling region and, therefore, an increased local pressure drop. The increase in flux, however, also causes an increase in the wall temperature in the nonboiling regions and, therefore, a decrease in pressure drop in these regions. The two effects apparently balance each other out (for the particular flux distribution of this investigation). The Reynolds number effect with local nucleate boiling is apparently a change in the balance between the two pressure-drop modes, the nonboiling effect becoming more dominant with decreasing Reynolds number.

## CONCLUSIONS

The possibilities of nozzle cooling at very high heat fluxes by forced-convection nucleate boiling of water has been investigated experimentally. The results may be summarized as follows:

1. Forced-convection nucleate boiling of water in axial flow may be successfully employed at very high local heat fluxes. Steady-state nucleate boiling was maintained at local heat fluxes up to 11,200 Btu/(sq ft)(sec).

2. Existing burnout prediction methods are not applicable to a flux distribution with large gradients such as that of a high-temperature flow nozzle.

3. The nonboiling forced-convection heat-transfer results are well represented by the Colburn equation with a modified coefficient.

4. The nucleate-boiling heat-transfer correlation of Forster and Greif represents the experimental heat-flux results quite well.

Lewis Research Center
National Aeronautics and Space Administration
Cleveland, Ohio, February 6, 1962

# APPENDIX A

## SYMBOLS

| | |
|---|---|
| A | area |
| b | effective circumference, eq. (B21a), or plate width |
| $C_o$ | conversion factor from electrical power to heat |
| $c_p$ | specific heat at constant pressure |
| d | diameter |
| E | voltage drop |
| f | friction factor, eq. (7) |
| g | acceleration due to gravity |
| H | enthalpy |
| h | heat-transfer coefficient |
| I | current |
| k | thermal conductivity |
| $k_r$ | reference thermal conductivity, $0^\circ$ F |
| L | pressure-drop length |
| $l$ | one-half test-section heated length |
| Nu | Nusselt number |
| Pr | Prandtl number |
| p | pressure |
| $\Delta p$ | pressure drop |
| Q | heat flux |
| q | heat flux per unit area |
| R | electrical resistance |

| | |
|---|---|
| Re | Reynolds number (based on diameter) |
| r | radius |
| St | Stanton number |
| s | heated length to burnout |
| T | temperature |
| t | wall thickness |
| u | temperature parameter, eq. (B8) |
| v | velocity |
| w | flow rate |
| x | rectangular coordinate |
| y | axial coordinate |
| z | cylindrical coordinate |
| $\alpha$ | temperature coefficient of thermal conductivity |
| $\theta$ | cylindrical coordinate |
| $\theta_o$ | angle defining wall thickness variation |
| $\eta$ | cylindrical coordinate |
| $\rho$ | density |
| $\sigma$ | average electrical resistivity |

Subscripts:

| | |
|---|---|
| b | local bulk |
| bo | burnout |
| c | cross section or conduction |
| e | electrical |
| f | film ($T_f = (T_w + T_b)/2$) |

| | |
|---|---|
| i | inside wall |
| in | inlet bulk |
| o | outside wall |
| out | outlet bulk |
| s | stagnation (air) |
| sat | saturation |
| w | wall, heat-transfer side |
| 0 | minimum-heat-flux location, $y = \pm l$ |
| 1 | maximum-heat-flux location, $y = 0$ |

# APPENDIX B

## TEMPERATURE DISTRIBUTION IN A RESISTANCE-HEATED TUBE WITH A LINEAR VARIATION IN WALL THICKNESS

First consider a resistance-heated flat plate with a linear wall thickness variation as shown in sketch (a):

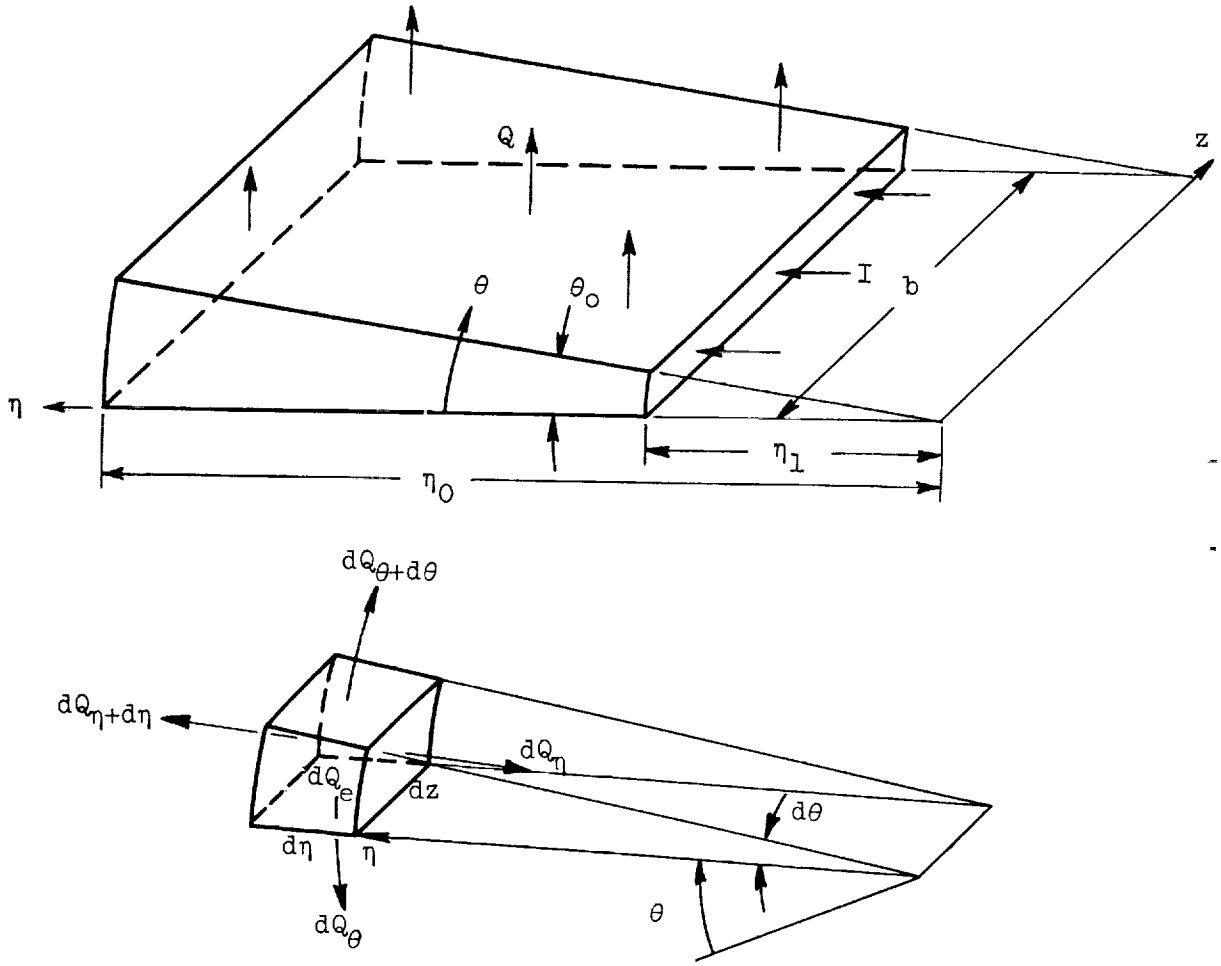


(a)

In a cylindrical coordinate system, the heat leaving a differential volume of the plate is given by

$$\left.\begin{aligned} dQ_\theta &= k \frac{\partial T}{\eta\, \partial\theta}\, d\eta\, dz \\ dQ_{\theta+d\theta} &= -\left[k \frac{\partial T}{\eta\, \partial\theta} + \frac{\partial}{\eta\, \partial\theta}\left(k \frac{\partial T}{\eta\, \partial\theta}\right)\eta\, d\theta\right] d\eta\, dz \\ dQ_\eta &= k \frac{\partial T}{\partial \eta}\, \eta\, d\theta\, dz \\ dQ_{\eta+d\eta} &= -\left[k \frac{\partial T}{\partial \eta} + \frac{\partial}{\partial \eta}\left(k \frac{\partial T}{\partial \eta}\right) d\eta\right](\eta + d\eta) d\theta\, dz \end{aligned}\right\} \quad \text{(B1)}$$

where $\eta$, $\theta$, and $z$ are the cylindrical coordinates (the plate is assumed isothermal in the z-direction). The heat generated within the differential volume is

$$dQ_e = C_o (I)^2_{dV} (R)_{dV} \quad \text{(B2)}$$

where

$$(I)_{dV} = I \frac{dA_c}{A_c} = I \frac{\eta\, d\theta\, dz}{\eta \theta_o b} \quad \text{(B3)}$$

($I$ is the total current through the plate and $(I)_{dV}$ is the fraction through $dV$) and

$$(R)_{dV} = \sigma \frac{d\eta}{dA_c} = \sigma \frac{d\eta}{\eta\, d\theta\, dz} \quad \text{(B4)}$$

The constant $C_o$ is the conversion factor from electrical power to heat. Therefore,

$$dQ_e = C_o I^2 \sigma \frac{d\eta\, d\theta\, dz}{\eta \theta_o^2 b^2} \quad \text{(B5)}$$

The heat balance for the volume is

$$dQ_e = dQ_\theta + dQ_{\theta+d\theta} + dQ_\eta + dQ_{\eta+d\eta}$$

and therefore the governing differential equation is

$$\frac{1}{\eta}\frac{\partial}{\partial\theta}\left(k\frac{\partial T}{\partial\theta}\right)+\eta\frac{\partial}{\partial\eta}\left(k\frac{\partial T}{\partial\eta}\right)+k\frac{\partial T}{\partial\eta}+C_o\frac{I^2\sigma}{\eta\theta_o^2b^2}=0 \tag{B6}$$

To eliminate the temperature variation of thermal conductivity, assume

$$k=k_r(1+\alpha T) \tag{B7}$$

and let

$$u=T\left(1+\frac{\alpha}{2}T\right) \tag{B8}$$

Therefore the governing differential equation becomes

$$\frac{\partial^2u}{\partial\eta^2}+\frac{1}{\eta}\frac{\partial u}{\partial\eta}+\frac{1}{\eta^2}\frac{\partial^2u}{\partial\theta^2}+C_o\frac{I^2\sigma}{k_r\theta_o^2b^2}\frac{1}{\eta^2}=0 \tag{B9}$$

Experimentally, one side of the plate (the side away from the coolant) may be considered as insulated and the temperature on that side is known. The boundary conditions are therefore

$$\left(\frac{\partial T}{\partial\theta}\right)_o=0 \quad \text{or} \quad \left(\frac{\partial u}{\partial\theta}\right)_o=0 \tag{B10}$$

$$T_o \text{ known} \quad \text{or} \quad u_o \text{ known}$$

where the subscript o indicates $\theta = 0$, the outside wall.

A Taylor series expansion about $u(\eta,0)$ yields

$$u(\eta,\theta)=u_o+\theta\left(\frac{\partial u}{\partial\theta}\right)_o+\frac{\theta^2}{2}\left(\frac{\partial^2u}{\partial\theta^2}\right)_o+\cdots \tag{B11}$$

But from the boundary conditions

$$\left(\frac{\partial u}{\partial\theta}\right)_o=0$$

and therefore

$$u(\eta,\theta)=u_o+\frac{\theta^2}{2}\left(\frac{\partial^2u}{\partial\theta^2}\right)_o \tag{B12}$$

when higher terms are neglected. From the governing differential equation

$$\frac{\partial^2 u}{\partial \theta^2} = -\eta^2 \frac{\partial^2 u}{\partial \eta^2} - \eta \frac{\partial u}{\partial \eta} - C_o \frac{I^2 \sigma}{k_r \theta_o^2 b^2}$$

and thus the equation for the temperature distribution in a flat plate with a linear variation in wall thickness is

$$u(\eta, \theta) = u_o - \frac{\theta^2}{2} \left[ \eta^2 \left( \frac{\partial^2 u}{\partial \eta^2} \right)_o + \eta \left( \frac{\partial u}{\partial \eta} \right)_o + C_o \frac{I^2 \sigma}{k_r \theta_o^2 b^2} \right] \tag{B13}$$

where $\theta_o$ is small. The temperature drop through the wall at any $\eta$ is therefore

$$u_o - u(\eta, \theta_o) = C_o \frac{I^2 \sigma}{2 k_r b^2} + \frac{\eta \theta_o^2}{2} \left[ \eta \left( \frac{\partial^2 u}{\partial \eta^2} \right)_o + \left( \frac{\partial u}{\partial \eta} \right)_o \right] \tag{B14}$$

(This is also the equation for the inside or coolant-side wall temperature distribution).

The differential equation for a resistance-heated tube with a linear variation in wall thickness (fig. 6) is not amenable to solution. A reasonable approach to obtain an approximate solution is the use of the previous plate solution where the plate width is a representative local circumference of the tube. The required plate width in terms of tube geometry may be obtained from the solutions for the temperature drops through a resistance-heated constant-wall-thickness flat plate and constant-wall-thickness tube. The solution for the temperature distribution in an electrically heated flat plate (sketch (b)) is

$$u(x) = u(o) - \frac{C_o}{2} \frac{I^2 \sigma}{k_r t^2 b^2} x^2 \tag{B15}$$

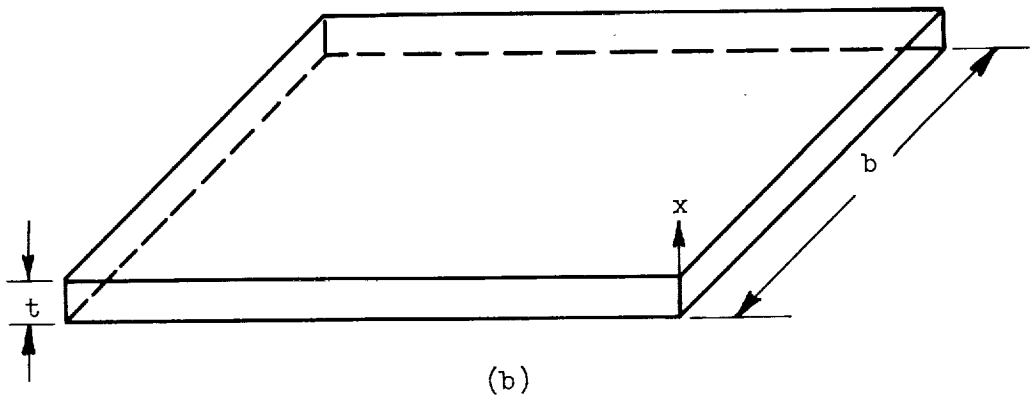


(b)

where

$$\left(\frac{du}{dx}\right)_{x=0} = 0$$

The total drop through the wall is therefore

$$u(o) - u(t) = \frac{C_o}{2} \frac{I^2\sigma}{k_r b^2} \tag{B16}$$



The solution for the temperature distribution in a resistance-heated constant-wall-thickness tube as shown in sketch (c) is

$$u(r) = u(r_o) - \frac{C_o}{4} \frac{I^2\sigma}{k_r\left[\pi t(2r_i + t)\right]^2} r_o^2 \left(\frac{r^2}{r_o^2} + 2 \ln \frac{r_o}{r} - 1\right) \tag{B17}$$

where

$$\left(\frac{\partial u}{\partial r}\right)_{r=r_o} = 0$$

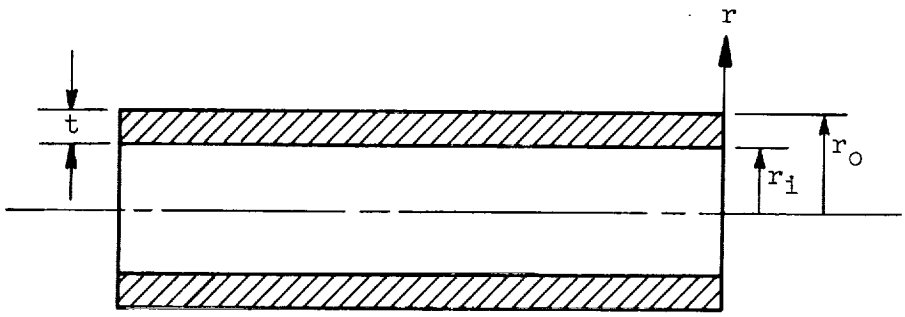


(c)

The total drop through the wall is therefore

$$u(r_o) - u(r_i) = \frac{C_o}{4} \frac{I^2\sigma}{k_r\left[\pi t(2r_i + t)\right]^2} r_o^2 \left(\frac{r_i^2}{r_o^2} + 2 \ln \frac{r_o}{r_i} - 1\right) \tag{B18}$$

The condition that the two configurations at equal outside wall temperatures have the same coolant-side wall temperature requires that

$$u_p(o) - u_p(t) = u_t(r_o) - u_t(r_i) \tag{B19}$$

where the subscripts indicate plate and tube. Therefore,

$$\frac{C_o}{2}\frac{I^2\sigma}{k_r b^2} = \frac{C_o}{4}\frac{I^2\sigma}{k_r[\pi t(2r_i + t)]^2} r_o^2\left(\frac{r_i^2}{r_o^2} + 2\ln\frac{r_o}{r_i} - 1\right) \tag{B20}$$

which reduces to

$$b^2 = \frac{2[\pi t(2r_i + t)]^2}{r_o^2\left(\frac{r_i^2}{r_o^2} + 2\ln\frac{r_o}{r_i} - 1\right)} \tag{B21}$$

where $b$ is the required width of a flat plate, which when applied in the flat-plate solution will yield results for a tube. Therefore, the approximate solution for the temperature drop in a resistance-heated tube (fig. 6) is given by equation (B14):

$$u_o - u(\eta, \theta_o) = C_o\frac{I^2\sigma}{2k_r b^2} + \frac{\eta\theta_o^2}{2}\left[\eta\left(\frac{\partial^2 u}{\partial\eta^2}\right)_o + \left(\frac{\partial u}{\partial\eta}\right)_o\right] \tag{B14}$$

where $b^2$ is given by equation (B21) applied locally, which in terms of appropriate variables is

$$b^2 = \frac{2[\pi\eta\theta_o(\eta\theta_o + d_i)]^2}{r_o^2\left[\left(\frac{r_i}{r_o}\right)^2 + 2\ln\frac{r_o}{r_i} - 1\right]} \tag{B21a}$$

and where

$$r_o = r_i + \eta\theta_o$$

Therefore, the axial coolant-side wall temperature distribution is available from the measured outside wall temperature distribution. The solution reduces to that for a constant-wall-thickness tube when the derivative terms are set equal to zero.

## APPENDIX C

## HEAT-TRANSFER RELATIONS FOR A RESISTANCE-HEATED TUBE WITH A LINEAR VARIATION IN WALL THICKNESS

The resistance of an increment of length $d\eta$ of the linearly tapered tube shown in figure 6 is

$$dR = \frac{\sigma \, d\eta}{A_c}$$

where

$$A_c = \pi\eta\theta_o(d_i + \eta\theta_o)$$

and thus

$$dR = \frac{\sigma}{\pi\theta_o} \frac{d\eta}{\eta(\eta\theta_o + d_i)} \tag{C1}$$

The total resistance of the tube is

$$R = \frac{\sigma}{\pi\theta_o} \int_{\eta_1}^{\eta_o} \frac{d\eta}{\eta(\eta\theta_o + d_i)} = \frac{\sigma}{\pi d_i \theta_o} \ln \left[ \left( \frac{\eta_o}{\eta_1} \right) \left( \frac{\eta_1\theta_o + d_i}{\eta_o\theta_o + d_i} \right) \right] \tag{C2}$$

The heat generated in the small-length increment is

$$dQ = C_o I^2 \, dR$$

and therefore

$$Q = C_o \frac{I^2\sigma}{\pi d_i \theta_o} \ln \left[ \left( \frac{\eta_o}{\eta_1} \right) \left( \frac{\eta_1\theta_o + d_i}{\eta_o\theta_o + d_i} \right) \right] \tag{C4}$$

If axial heat conduction is neglected and the outside wall ($\theta = 0$) is insulated, the incremental heat into the coolant stream is

$$dQ = q \, dA_w$$

where $dQ$ is the heat generated (eq. (C3)), $q$ is the local value of heat flux, and

$$dA_w = \pi d_i \, d\eta$$

Therefore the local heat flux, neglecting conduction, is

$$q = C_o \frac{I^2\sigma}{\pi^2 d_i \eta\theta_o(\eta\theta_o + d_i)} \tag{C5}$$



The experimental temperature distribution is nonuniform, and therefore corrections must be made on equation (C5) to account for axial conduction. The heat gained or lost by a volume $d\eta$ wide (fig. 6) due to axial conduction is found to be

$$dQ_c = -\pi\eta\theta_o(\eta\theta_o + d_i)k_r\left(\frac{1}{\eta}\frac{d\bar{u}}{d\eta} + \frac{d^2\bar{u}}{d\eta^2}\right)d\eta \tag{C6}$$

where $\bar{u}$ is the average value of the temperature parameter at $\eta$ based on wall cross-sectional area and is given by

$$\bar{u} = u_o - \frac{\frac{3}{2}\eta\theta_o + d_i}{\eta\theta_o + d_i}\left\{\frac{C_o}{6}\frac{I^2\sigma}{k_r b^2} + \frac{\eta\theta_o^2}{6}\left[\eta\left(\frac{\partial^2 u}{\partial\eta^2}\right)_o + \left(\frac{\partial u}{\partial\eta}\right)_o\right]\right\} \tag{C7}$$

where $b^2$ is given by equation (B21a). Therefore, from equations (C3) and (C6) the net heat into the coolant stream assuming an insulated outside wall is given by

$$dQ_i = C_o\frac{I^2\sigma}{\pi\theta_o}\frac{d\eta}{\eta(\eta\theta_o + d_i)} - \pi\eta\theta_o(\eta\theta_o + d_i)\,k_r\left(\frac{1}{\eta}\frac{\partial\bar{u}}{\partial\eta} + \frac{\partial^2\bar{u}}{\partial\eta^2}\right)d\eta \tag{C8}$$

The local value of the heat flux into the coolant stream is therefore

$$q_i = C_o\frac{I^2\sigma}{\pi^2 d_i\eta\theta_o(\eta\theta_o + d_i)} - \frac{\eta\theta_o(\eta\theta_o + d_i)}{d_i}k_r\left(\frac{1}{\eta}\frac{d\bar{u}}{d\eta} + \frac{d^2\bar{u}}{d\eta^2}\right) \tag{C9}$$

where $\bar{u}$ is given by equation (C7).

Assuming that the heat transferred to the stream by an incremental length $d\eta$ (fig. 6) goes into increasing the bulk temperature across that length, the bulk temperature distribution is given by

$$(T_b)_\eta = T_{in} + \Delta T \left\{ 1 - \frac{\ln \left[ \left( \frac{\eta}{\eta_1} \right) \left( \frac{\eta_1 \theta_o + d_i}{\eta \theta_o + d_i} \right) \right]}{\ln \left[ \left( \frac{\eta_o}{\eta_1} \right) \left( \frac{\eta_1 \theta_o + d_i}{\eta_o \theta_o + d_i} \right) \right]} \right\} \qquad (C10)$$

where the flow is in the direction of decreasing $\eta$ and $\Delta T$ is the temperature rise over the heated length $l$.

## REFERENCES


1. Sutton, G. P.: Rocket Propulsion Elements. Second ed, John Wiley & Sons, Inc., 1956.

2. John, Richard R., and Bade, William L.: Recent Advances in Electric Arc Plasma Generation Technology. ARS Jour., vol. 31, no. 1, Jan. 1961, pp. 4-17.

3. Jack, John R.: Regenerative and Radiation Cooling of Electrothermal Thrust Generators. Paper 61-97-1791, Am. Rocket Soc., Inc., 1961.

4. Jens, W. H., and Lottes, P. A.: Analysis of Heat Transfer, Burnout, Pressure Drop and Density Data for High-Pressure Water. ANL-4627, Argonne Nat. Lab., May 1, 1951.

5. Kreith, Frank, and Summerfield, Martin: Heat Transfer to Water at High Flux Densities with and without Surface Boiling. Trans. ASME, vol. 71, no. 7, Oct. 1949, pp. 805-815.

6. McAdams, W. H., et al.: Heat Transfer at High Rates to Water with Surface Boiling. Ind. and Eng. Chem., vol. 41, no. 9, Sept. 1949, pp. 1945-1953.

7. McAdams, William H.: Heat Transmission. Third ed., McGraw-Hill Book Co., Inc., 1954.

8. Forster, K., and Greif, R.: Heat Transfer to a Boiling Liquid - Mechanism and Correlations. Jour. Heat Transfer, ser. C., vol. 81, no. 1, Feb. 1959, pp. 43-53.

9. Lowdermilk, Warren H., Lanzo, Chester D., and Siegel, Byron L.: Investigation of Boiling Burnout and Flow Stability for Water Flowing in Tubes. NACA TN 4382, 1958.

10. Gambill, W. R., and Greene, N. D.: Boiling Burnout with Water in Vortex Flow. Chem. Eng. Prog., vol. 54, no. 10, Oct. 1958, pp. 68-76.

11. Gambill, W. R., Bundy, R. D., and Wansbrough, R. W.: Heat Transfer, Burnout, and Pressure Drop for Water in Swirl Flow Through Tubes with Internal Twisted Tapes. Preprint 22, Am. Inst. Chem. Eng., 1960.

12. Bernath, Louis: Prediction of Heat Transfer Burnout. Preprint 8, Am. Inst. Chem. Eng., 1955.

13. Sonnemann, G.: A Method of Correlating Burnout Heat Flux Data. Nuclear Sci. Eng., vol. 5, no. 4, Apr. 1959, pp. 242-247.

14. Reshotko, Eli, and Tucker, Maurice: Approximate Calculation of the Compressible Turbulent Boundary Layer with Heat Transfer and Arbitrary Pressure Gradient. NACA TN 4154, 1957.

15. Lucks, C. F., et al.: The Experimental Measurement of Thermal Conductivities, Specific Heats, and Densities of Metallic, Transparent, and Protector Materials, pt. I. TR 6145, WADC, Feb. 1951.

16. Anon.: Engineering Properties of Inconel and Inconel "X". Tech. Bull. T-7, International Nickel Co., Sept. 1959.

17. Hartnett, J. P., Eckert, E. R. G., Birkebak, Roland, and Sampson, R. L.: Simplified Procedures for the Calculation of Heat Transfer to Surfaces with Nonuniform Temperatures. TR 56-373, WADC, Dec. 1956.

18. Rohsenow, W. M., and Clark, J. A.: Heat Transfer and Pressure Drop Data for High Heat Flux Densities to Water at High Subcritical Pressures. Heat Transfer and Fluid Mech. Inst., 1951, pp. 193-253. 269-270.

TABLE I. - HEAT-TRANSFER RESULTS AT MAXIMUM-HEAT-FLUX LOCATION y = 0

| Test-section number | Heated length, $2l$, in. | Flow rate, $\rho v$, $\frac{lb}{(sq\ ft)(sec)}$ | Velocity, $v_{in}$, ft/sec | Heat flux, $q_l$, $\frac{Btu}{(sq\ ft)(sec)}$ | Bulk temperature, $T_b$, $^oF$ | Wall temperature, $T_w$, $^oF$ | Pressure, $p_l$, $\frac{lb}{sq\ in.\ abs}$ | Comments |
|---|---|---|---|---|---|---|---|---|
| 2 | 5.50 | $0.93\times10^4$ | 149 | 5,200 | 89 | 492 | 167 | |
| | | .94 | 151 | 5,200 | 95 | 520 | 167 | |
| | | 1.27 | 204 | 4,200 | 81 | 403 | 294 | |
| | | 1.08 | 174 | 4,210 | 83 | 412 | 220 | |
| | | .94 | 151 | 4,210 | 86 | 438 | 163 | |
| | | .78 | 125 | 4,220 | 89 | 460 | 116 | |
| | | .63 | 101 | 4,210 | 96 | 477 | 96 | |
| | | .45 | 73 | 4,210 | 105 | 494 | 69 | |
| | | .78 | 125 | 1,960 | 83 | 320 | --- | |
| | | .78 | 125 | 5,950 | 107 | 530 | 125 | |
| | | 1.27 | 204 | 1,960 | 88 | 265 | --- | |
| | | 1.27 | 204 | 4,080 | 96 | 415 | 307 | |
| | | 1.26 | 203 | 5,950 | 103 | 490 | 294 | |
| | | 1.26 | 203 | 7,500 | 106 | 500 | 296 | |
| | | .78 | 125 | 4,090 | 86 | 460 | 123 | |
| | | .78 | 126 | 4,090 | 85 | 448 | 123 | |
| | | .93 | 150 | 5,200 | 87 | 492 | 170 | |
| 3 | 5.50 | $0.93\times10^4$ | 150 | 1,990 | 93 | 309 | 139 | |
| | | 1.25 | 201 | 520 | 80 | 140 | 236 | |
| | | 1.25 | 201 | 1,040 | 82 | 198 | 233 | |
| | | 1.25 | 201 | 1,480 | 85 | 229 | 232 | |
| | | 1.25 | 201 | 2,020 | 87 | 275 | 231 | |
| | | 1.25 | 202 | 2,570 | 92 | 308 | 229 | |
| | | 1.25 | 202 | 3,010 | 94 | 337 | 229 | |
| | | 1.25 | 202 | 4,070 | 99 | 386 | 230 | |
| | | .63 | 102 | 510 | 83 | 172 | 243 | |
| | | .63 | 102 | 1,030 | 85 | 253 | 235 | |
| | | .63 | 102 | 1,530 | 88 | 313 | 234 | |
| | | 1.25 | 201 | 4,110 | 98 | 427 | 228 | |
| | | .95 | 153 | 4,090 | 102 | 456 | 223 | |
| | | .64 | 103 | 4,110 | 111 | 515 | 243 | |
| | | .93 | 150 | 6,130 | 113 | 516 | 135 | |
| | | .94 | 151 | 6,080 | 116 | 524 | 196 | |
| | | .93 | 150 | 6,080 | 116 | 538 | 250 | |
| | | .94 | 152 | 6,100 | 117 | 511 | 135 | |
| | | .93 | 149 | 6,120 | 108 | 530 | 192 | |
| | | 1.25 | 201 | 2,090 | 93 | 285 | 231 | |
| | | 1.25 | 201 | 4,100 | 100 | 409 | 229 | |
| | | 1.25 | 202 | 6,130 | 93 | 467 | 232 | |
| | | 1.25 | 202 | 8,060 | 95 | 508 | 234 | |
| | | .96 | 154 | 7,960 | [a]98 | --- | [a]234 | Maximum steady-state nucleate boiling |
| | | .96 | 154 | 8,040 | [a]98 | --- | [a]234 | Failure |
| | | [b].96 | [b]154 | [b]8,000 | [b]98 | --- | [b]234 | Burnout |
| 7 | 1.50 | $1.25\times10^4$ | 202 | 11,200 | [a]83 | --- | [a]220 | Maximum steady-state nucleate boiling |
| | | 1.25 | 202 | 11,700 | [a]83 | --- | [a]220 | Failure |
| | | [b]1.25 | [b]202 | [b]11,450 | [b]83 | --- | [b]220 | Burnout |
| 8 | 1.50 | $1.26\times10^4$ | 203 | 10,700 | [a]88 | --- | [a]195 | Maximum steady-state nucleate boiling |
| | | 1.26 | 203 | 11,500 | [a]88 | --- | [a]195 | Failure |
| | | [b]1.26 | [b]203 | [b]11,100 | [b]88 | --- | [b]195 | Burnout |

[a]Estimated values.

[b]Average of conditions at failure and maximum steady-state nucleate boiling.

TABLE II. - AXIAL DISTRIBUTION OF HEAT-TRANSFER PARAMETERS

| Test-section number | Heated length, $2l$, in. | Flow rate, $\rho v$, lb/(sq ft)(sec) | Velocity, $v_{in}$, ft/sec | Axial location, $y/l$ | Heat flux, $q$, Btu/(sq ft)(sec) | Bulk temperature, $T_b$, $^oF$ | Wall temperature, $T_w$, $^oF$ | Pressure, $p$, lb/sq in. abs |
|---|---|---|---|---|---|---|---|---|
| 3 | 5.50 | $0.63 \times 10^4$ | 102 | 0 | 1530 | 88 | 313 | --- |
| | | | | .27 | 739 | 92 | 238 | --- |
| | | | | .54 | 466 | 95 | 202 | --- |
| | | | | .69 | 385 | 96 | 197 | --- |
| | | | | .82 | 328 | 96 | 191 | --- |
| | | $1.25 \times 10^4$ | 202 | 0 | 8060 | 95 | 508 | 234 |
| | | | | .28 | 3880 | 106 | 421 | 209 |
| | | | | .54 | 2470 | 112 | 331 | --- |
| | | | | .69 | 2040 | 114 | 358 | --- |
| | | | | .82 | 1740 | 116 | 355 | --- |

TABLE III. - PRESSURE-DROP RESULTS

(a) No heat transfer

| Test-section number | Pressure-drop length, L, in. | Flow rate, $\rho v$, lb/(sq ft)(sec) | Velocity, $v_{in}$, ft/sec | Inlet temperature, $T_{in}$, °F | Pressure drop, $\Delta p$, lb/sq in. |
|---|---|---|---|---|---|
| 3 | 7.38 | $0.93 \times 10^4$ | 150 | 85 | 157 |
| | | 1.25 | 202 | 78 | 272 |
| | | 1.25 | 201 | 78 | 270 |
| | | 1.25 | 201 | 80 | 269 |
| | | 1.25 | 201 | 82 | 268 |
| | | 1.25 | 201 | 83 | 267 |
| | | 1.25 | 202 | 84 | 269 |
| | | 1.25 | 201 | 87 | 267 |
| | | .63 | 102 | 80 | 78 |
| | | .63 | 102 | 79 | 78 |
| | | .63 | 101 | 79 | 77 |
| | | 1.25 | 201 | 85 | 263 |
| | | .95 | 153 | 86 | 159 |
| | | .63 | 102 | 87 | 76 |
| | | .93 | 150 | 87 | 154 |
| | | .94 | 151 | 91 | 154 |
| | | .93 | 150 | 92 | 154 |
| | | .94 | 152 | 92 | 155 |
| | | .93 | 150 | 83 | 156 |
| | | 1.25 | 201 | 85 | 263 |
| | | 1.25 | 201 | 87 | 263 |
| | | 1.25 | 202 | 90 | 265 |
| | | 1.25 | 201 | 74 | 273 |
| | | 1.25 | 201 | 69 | 276 |
| 4 | 5.00 | .94 | 152 | 71 | 126 |
| 5 | 3.38 | .95 | 153 | 73 | 92 |
| 6 | 3.38 | .93 | 150 | 80 | 86 |
| | | .94 | 152 | 81 | 87 |

TABLE III. - Concluded. PRESSURE-DROP RESULTS

(b) Heat transfer

| Test-section number | Pressure drop, length, L, in., | Flow rate, $\rho v$, lb/(sq ft)(sec) | Velocity, $v_{in}$, ft/sec | Inlet temperature, $T_{in}$, $^{o}F$ | Heat flux, $q_l$, Btu/(sq ft)(sec) | Pressure drop, $\Delta p$, lb/sq in. |
|---|---|---|---|---|---|---|
| 3 | 7.38 | $0.93 \times 10^4$ | 150 | 85 | 1990 | 143 |
| | | 1.25 | 201 | 78 | 520 | 264 |
| | | 1.25 | 201 | 78 | 1040 | 258 |
| | | 1.25 | 201 | 80 | 1480 | 254 |
| | | 1.25 | 201 | 82 | 2020 | 250 |
| | | 1.25 | 202 | 83 | 2570 | 247 |
| | | 1.25 | 202 | 84 | 3010 | 246 |
| | | 1.25 | 202 | 87 | 4070 | 243 |
| | | .63 | 102 | 80 | 510 | 74 |
| | | .63 | 102 | 79 | 1030 | 70 |
| | | .63 | 102 | 79 | 1530 | 68 |
| | | 1.25 | 201 | 85 | 4110 | 235 |
| | | .95 | 153 | 86 | 4090 | 137 |
| | | .64 | 103 | 87 | 4110 | 64 |
| | | .93 | 150 | 87 | 6130 | 133 |
| | | .94 | 151 | 91 | 6080 | 134 |
| | | .93 | 150 | 92 | 6080 | 132 |
| | | .94 | 152 | 92 | 6100 | 136 |
| | | .93 | 149 | 83 | 6120 | 132 |
| | | 1.25 | 201 | 85 | 2090 | 243 |
| | | 1.25 | 201 | 87 | 4100 | 236 |
| | | 1.25 | 202 | 74 | 6130 | 235 |
| | | 1.25 | 202 | 69 | 8060 | 236 |

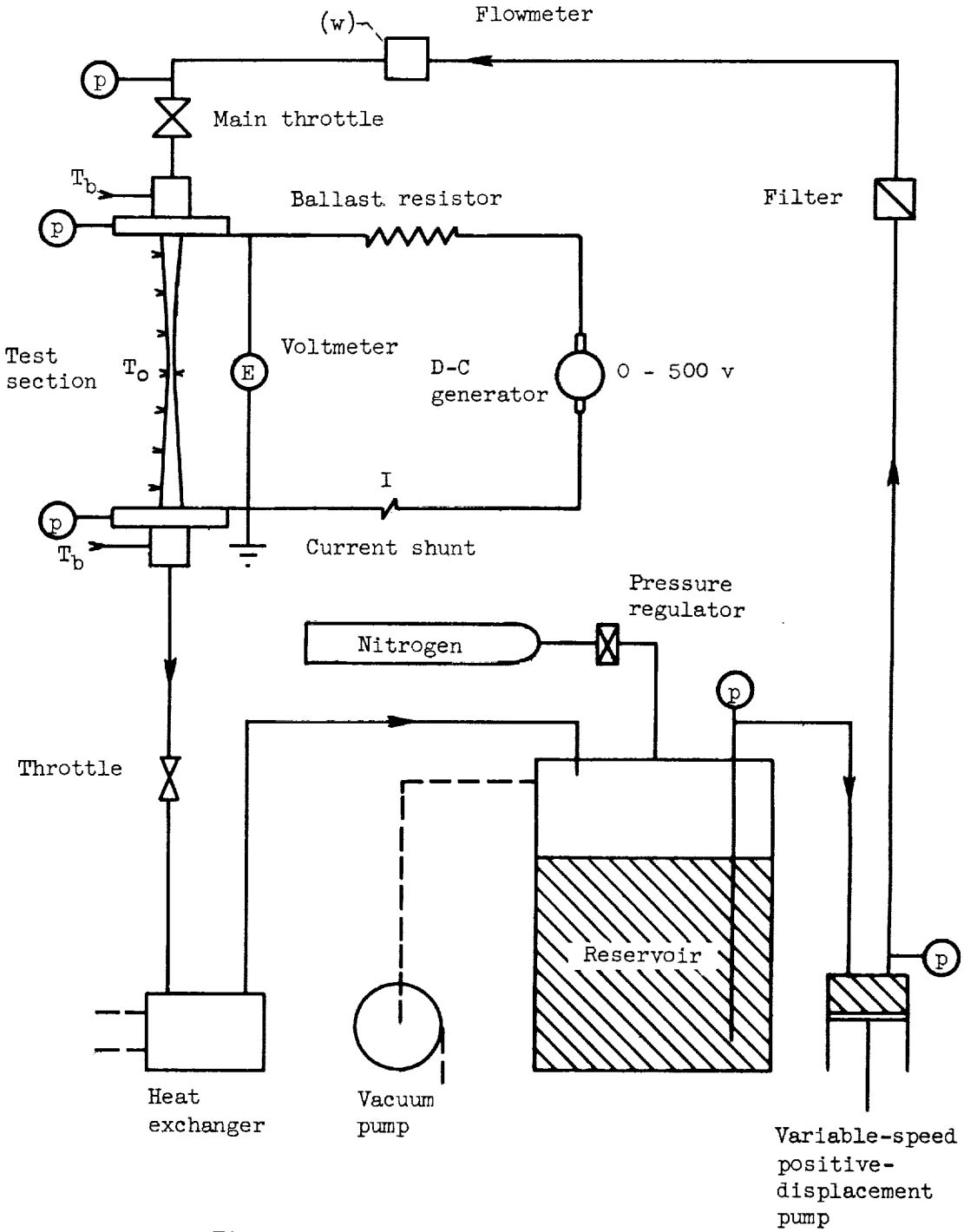


Figure 1. - Flow system and apparatus.

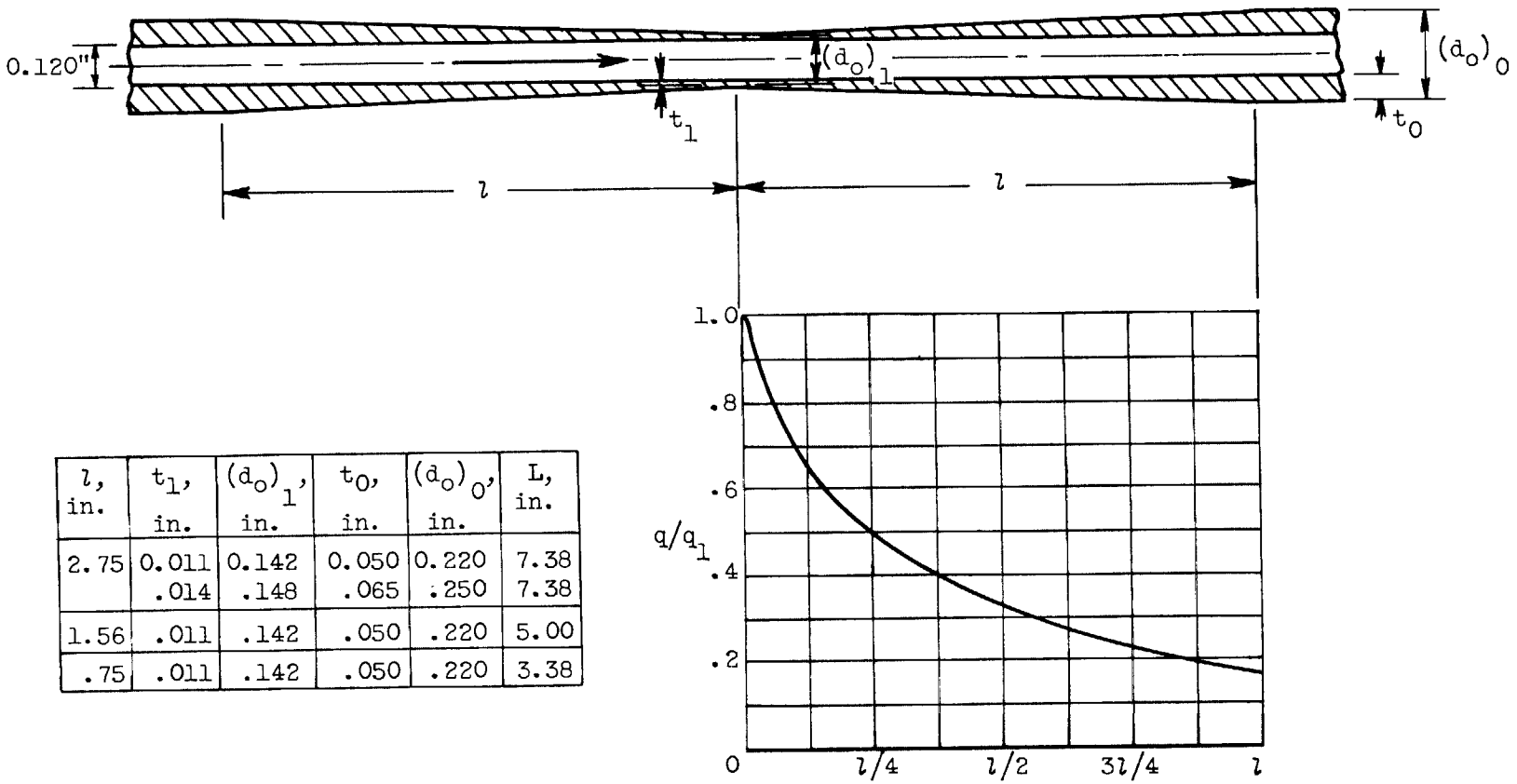


| l, in. | $t_1$, in. | $(d_o)_1$, in. | $t_o$, in. | $(d_o)_o$, in. | L, in. |
|---|---|---|---|---|---|
| 2.75 | 0.011 | 0.142 | 0.050 | 0.220 | 7.38 |
| | .014 | .148 | .065 | .250 | 7.38 |
| 1.56 | .011 | .142 | .050 | .220 | 5.00 |
| .75 | .011 | .142 | .050 | .220 | 3.38 |

Figure 2. - Test-section geometry and heat-flux distribution.

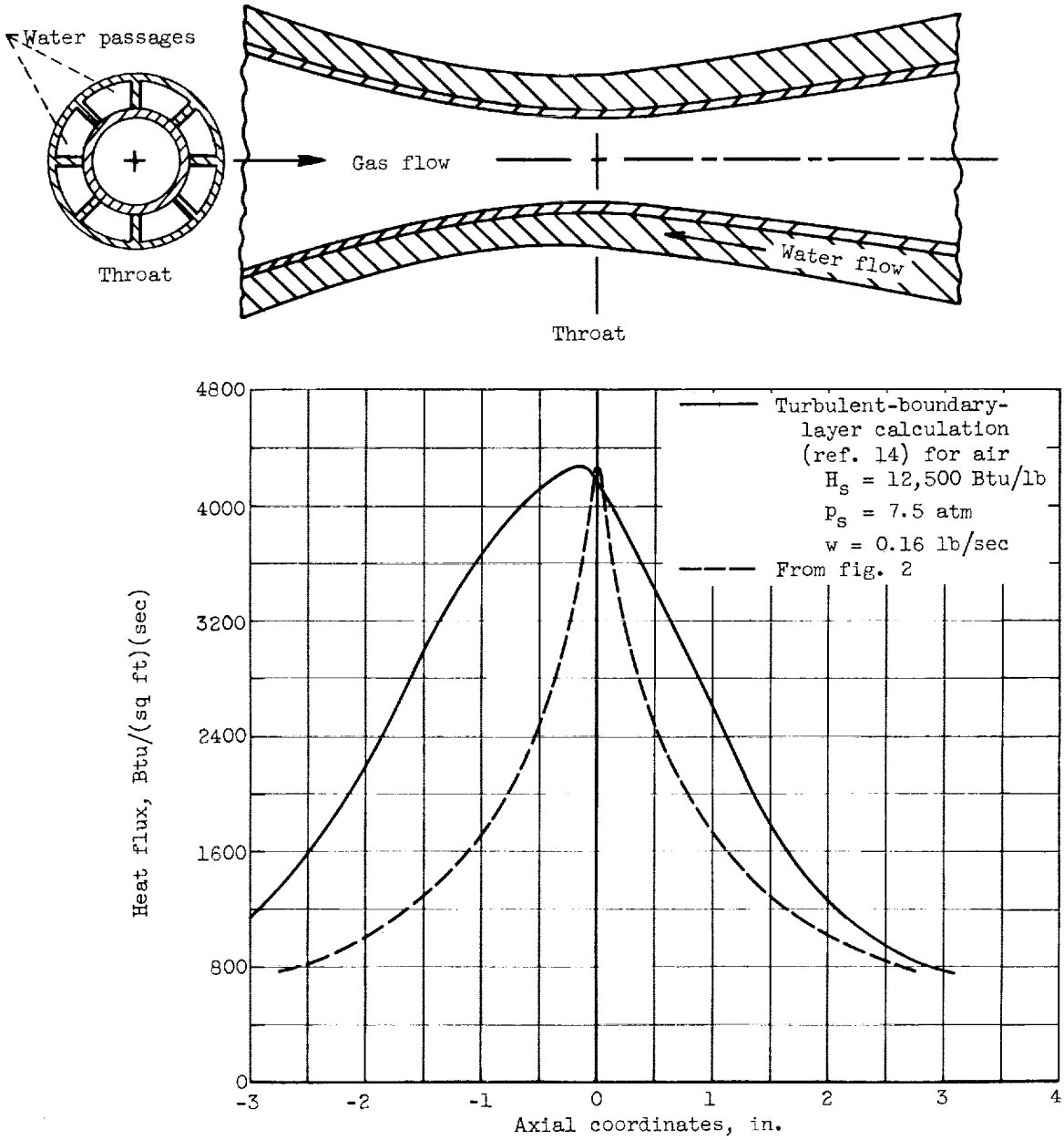


Figure 3. - Nozzle-throat section and heat-flux distribution for a preliminary configuration for Lewis Research Center Arc Tunnel.

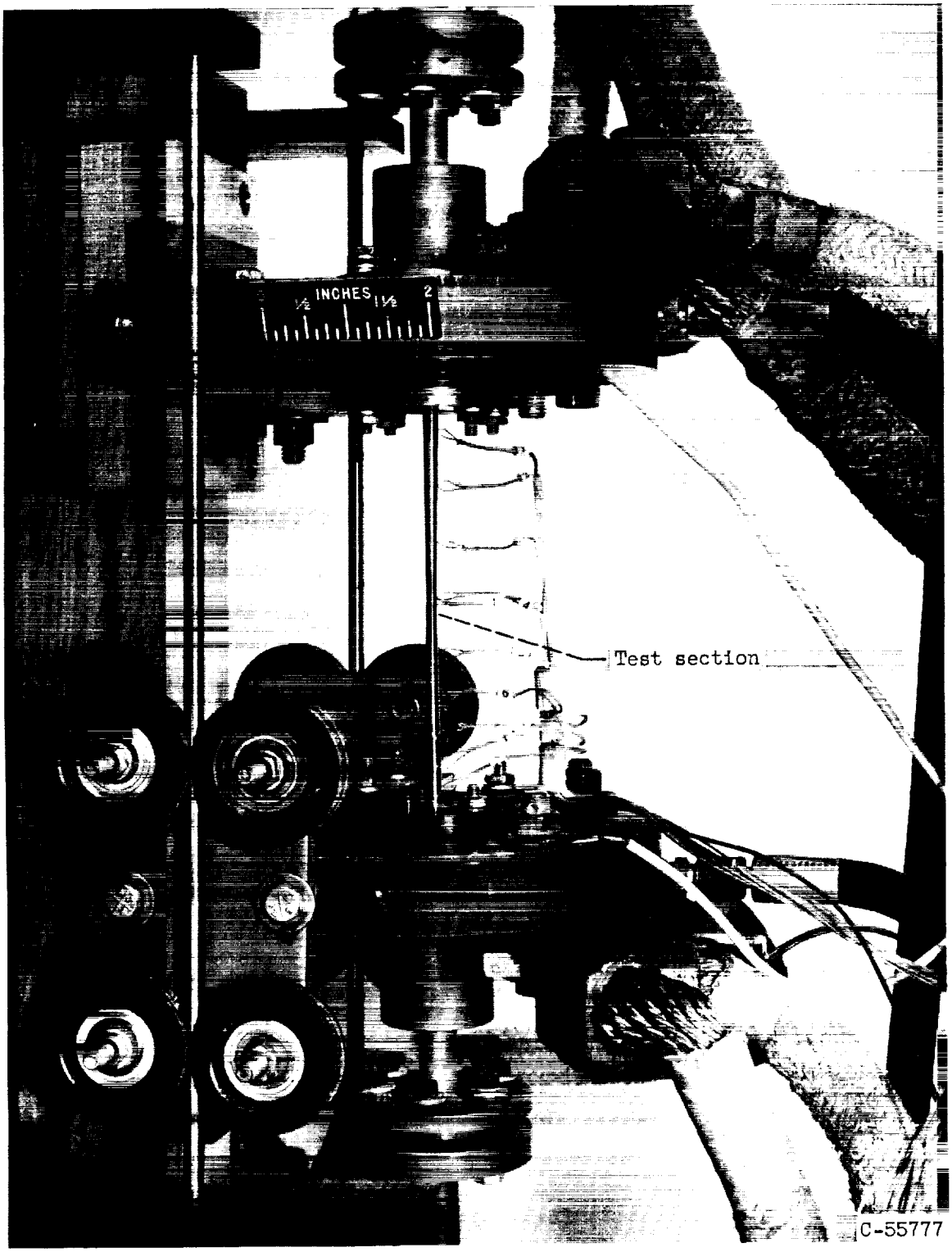


Figure 4. - Test rig.

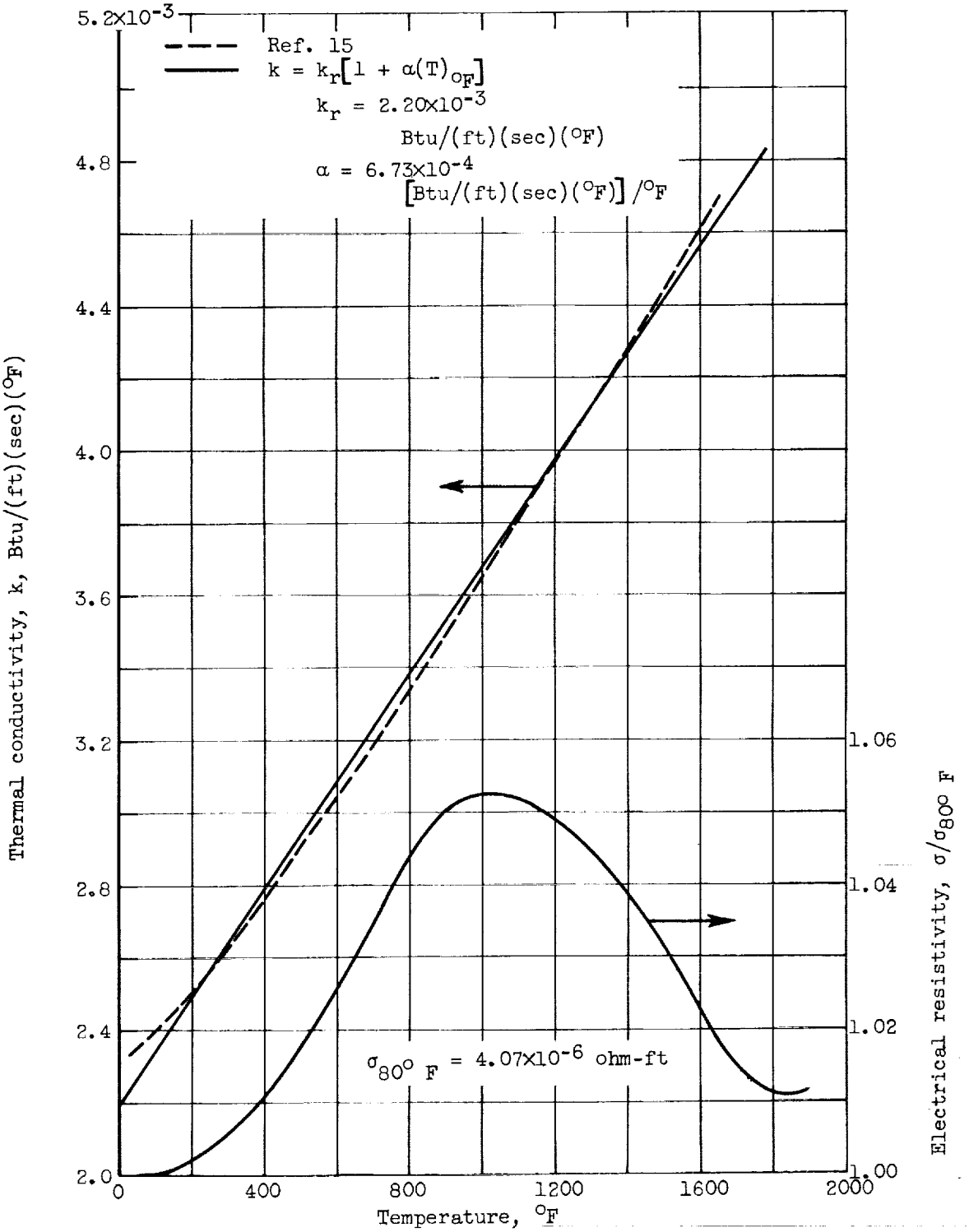


Figure 5. - Thermal conductivity and electrical resistivity of Inconel.

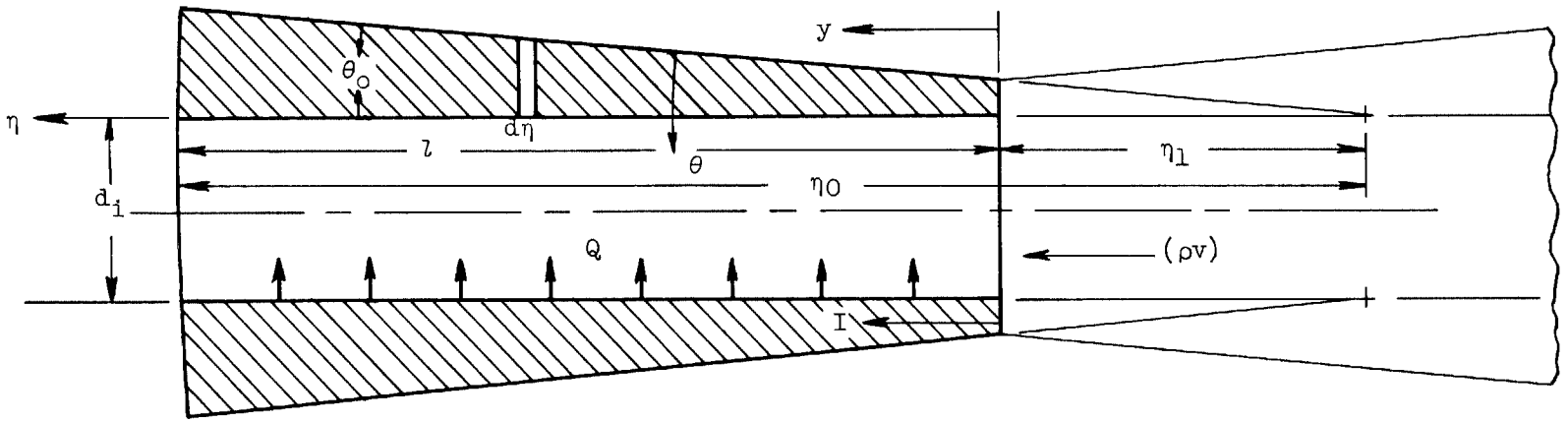


Figure 6. - Coordinate system and geometry variables for resistance-heated tube with linear variation in wall thickness.

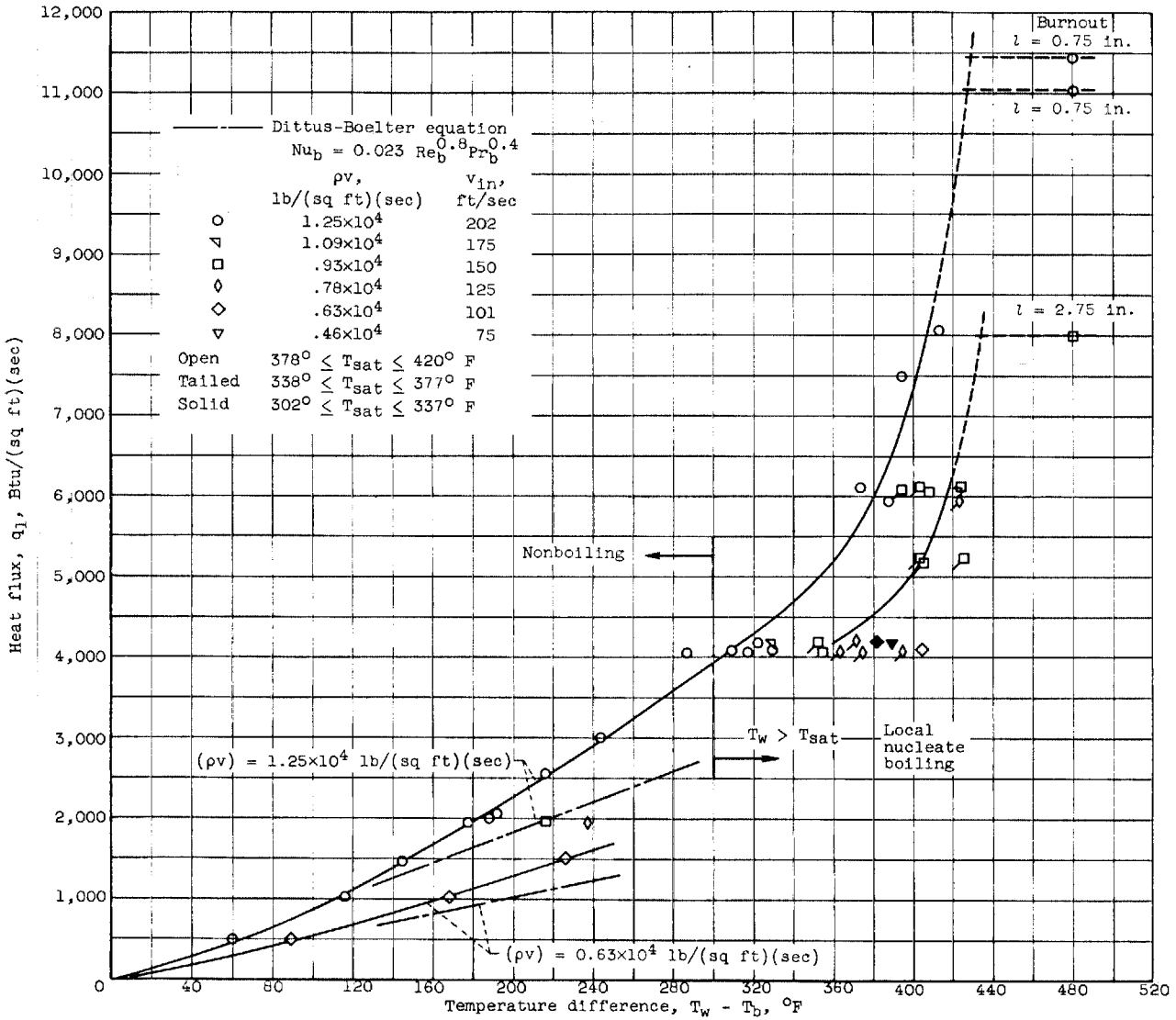


Figure 7. - Summary of heat-transfer results. 80° ≤ $T_b$ ≤ 117° F.

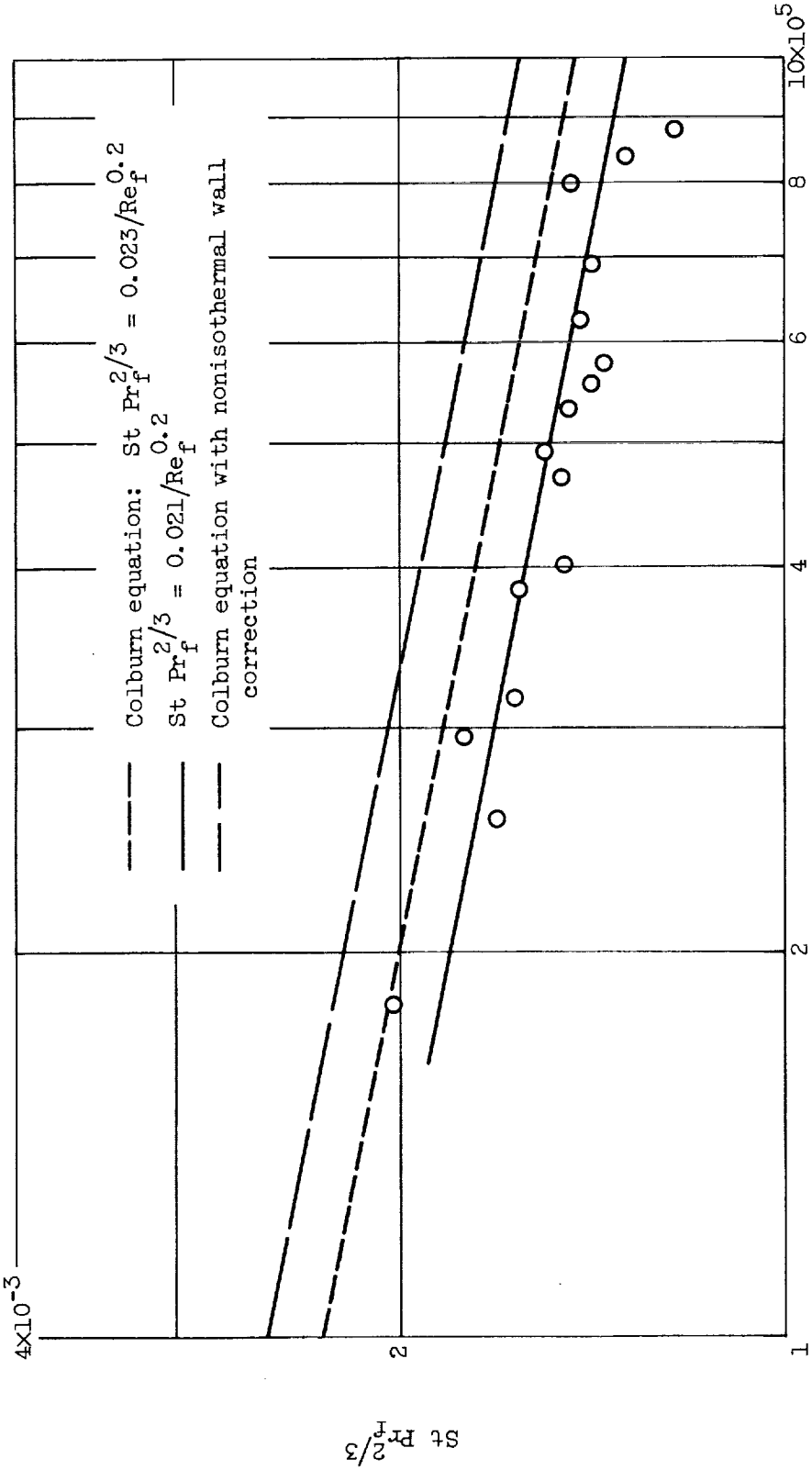


Figure 8. - Correlation of nonboiling forced-convection heat-transfer results at y = 0.

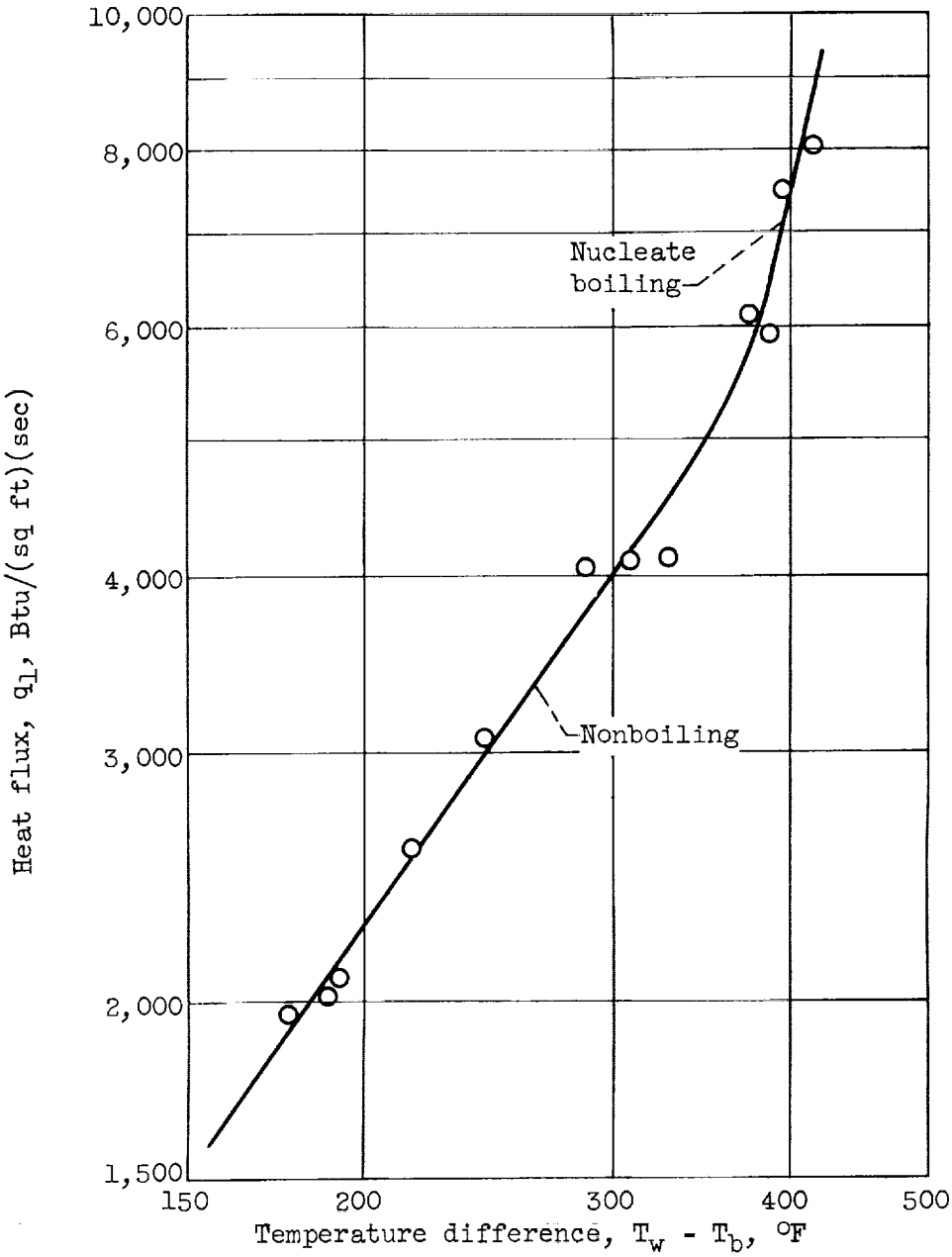


Figure 9. - Nonboiling and nucleate-boiling forced-convection heat transfer at high flow rate. $(\rho v) = 1.25 \times 10^4$ lb/(sq ft)(sec); $v_{in} = 202$ ft/sec; $T_{sat} - T_b = 305^\circ$ F; p = 260 lb/sq in. abs; $T_{sat} = 404^\circ$ F; $T_b = 99^\circ$ F.

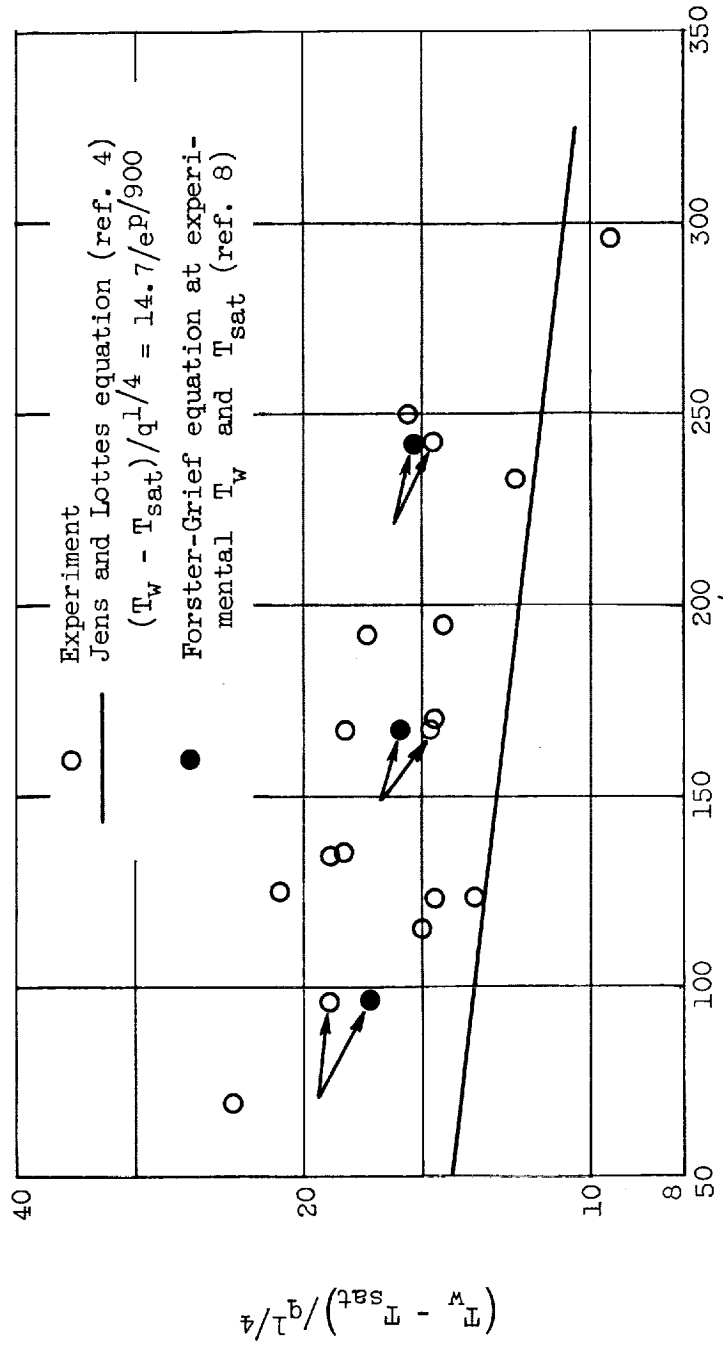


Figure 10. - Nucleate-boiling results in terms of the correlation of Jens and Lottes (ref. 4).

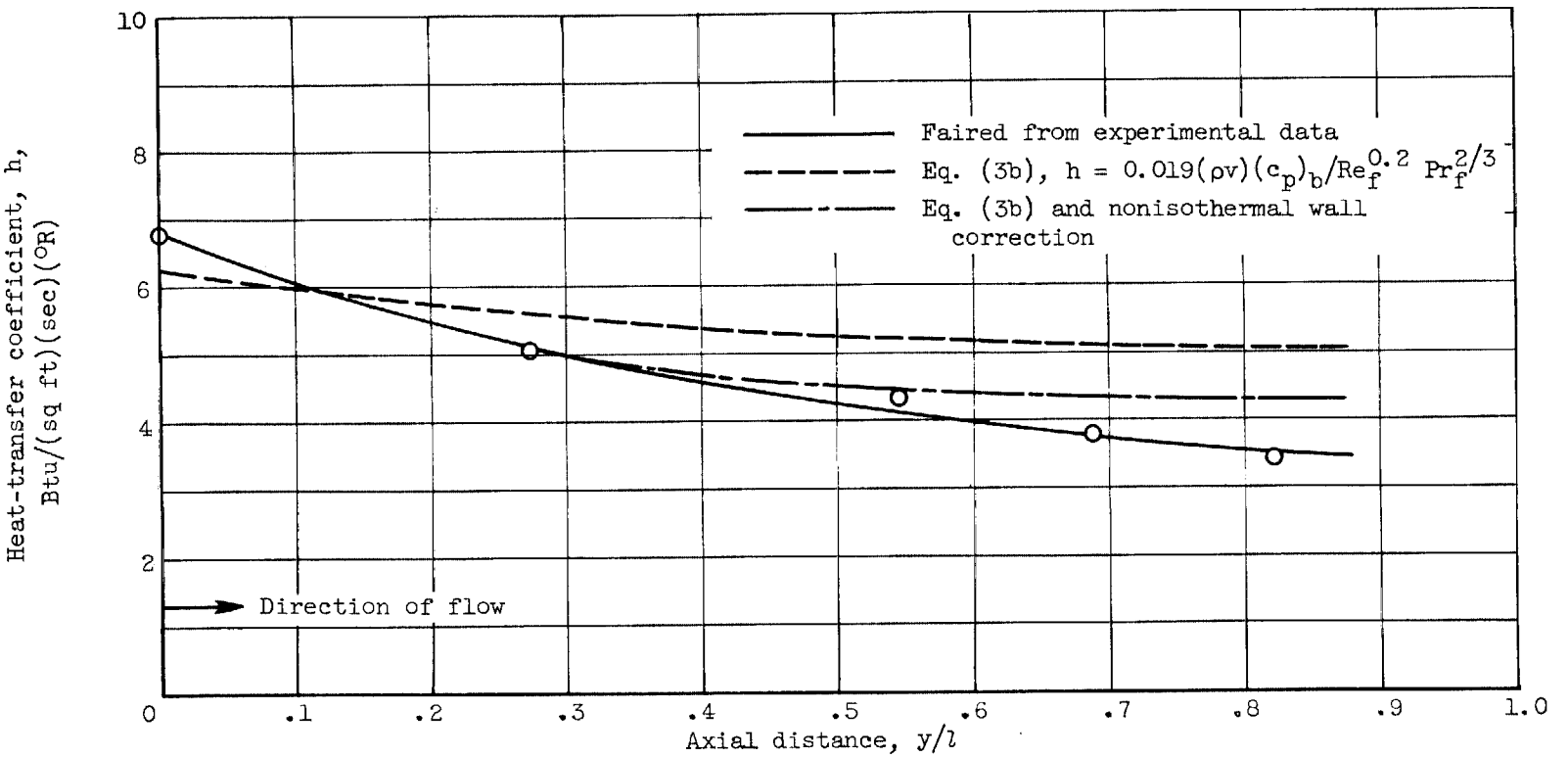


(a) Nonboiling. Heat flux, $q_l$, 1530 Btu/(sq ft)(sec) (axial distribution of fig. 2); velocity, $v_{in}$, 102 feet per second.

Figure 11. - Axial distribution of heat-transfer coefficient.

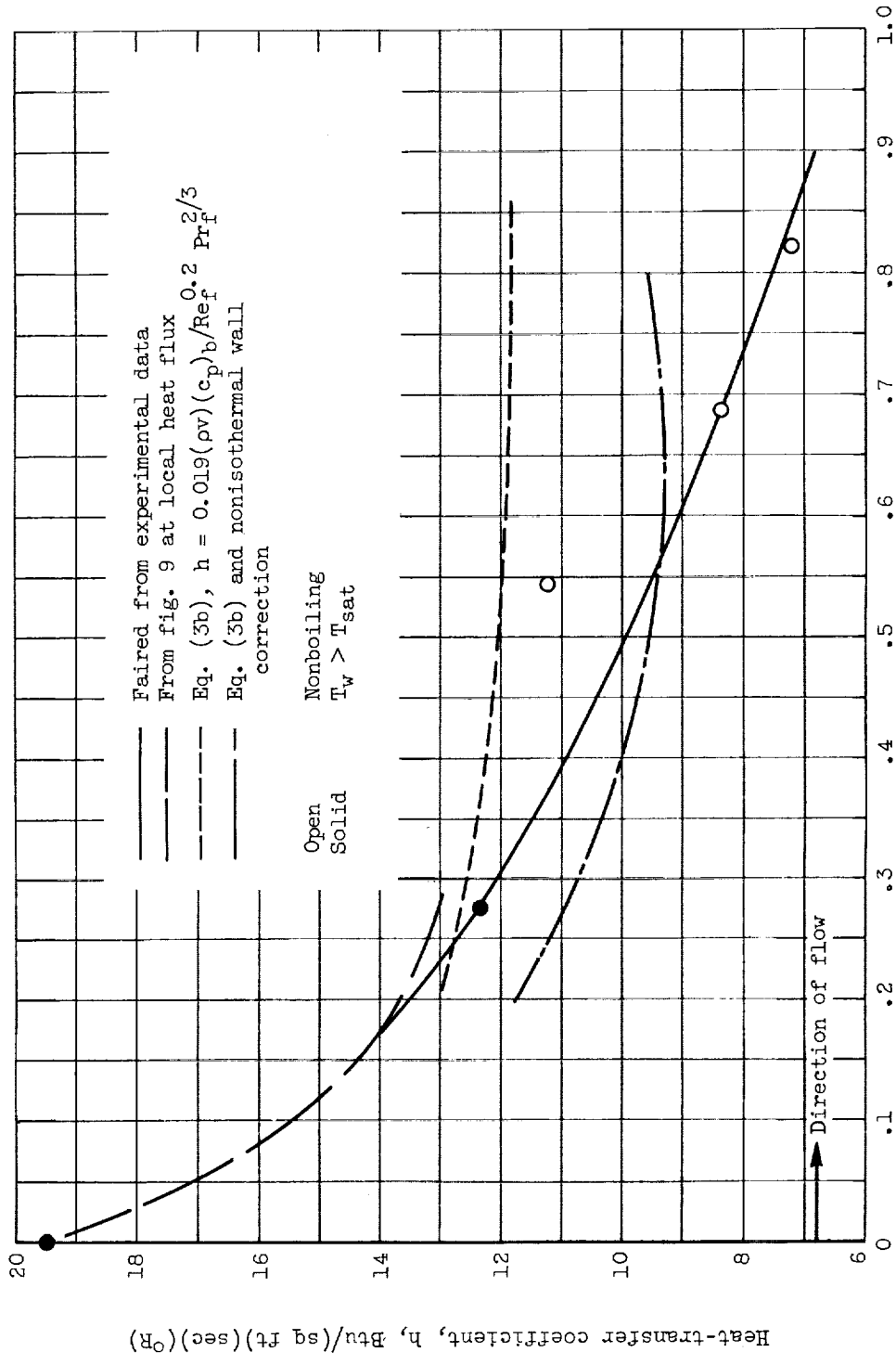


(b) Local nucleate boiling. Heat flux, $q_l$, 8060 Btu/(sq ft)(sec) (axial distribution of fig. 2); velocity, $v_{in}$, 202 feet per second.

Figure 11. - Concluded. Axial distribution of heat-transfer coefficient.

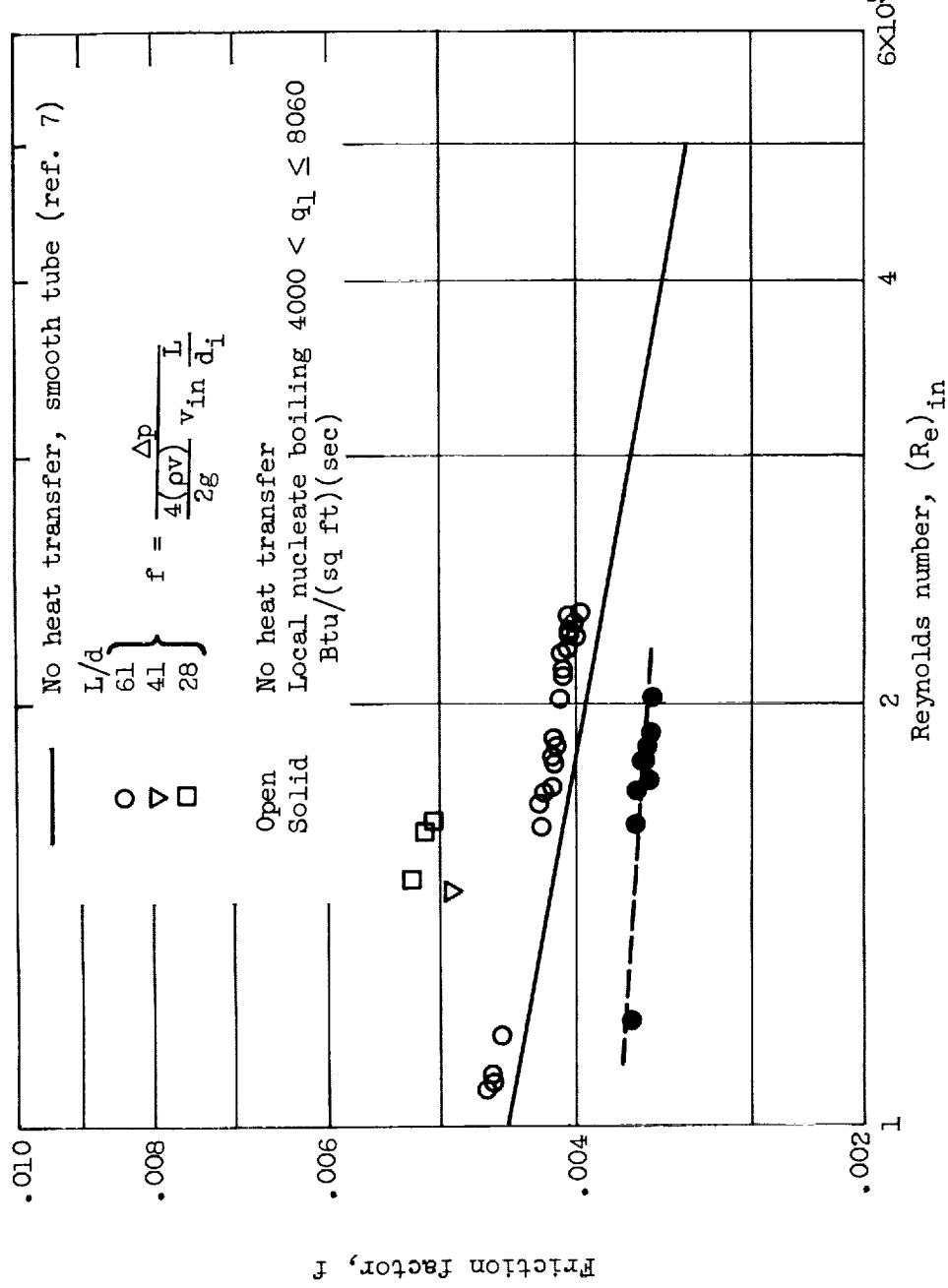


Figure 12. - Effective friction factor for flow with local nucleate boiling and flow with no heat transfer.



E-1215

NASA TN D-1214
National Aeronautics and Space Administration.
INVESTIGATION OF FORCED-CONVECTION NUCLEATE BOILING OF WATER FOR NOZZLE COOLING AT VERY HIGH HEAT FLUXES. John W. Schaefer and John R. Jack. May 1962. 46p. OTS price, $1.25. (NASA TECHNICAL NOTE D-1214)

The nonuniform axial heat-flux distribution typical of a very high temperature flow nozzle was simulated by resistance heating of variable-wall-thickness Inconel tubes. The coolant water flowed through the constant-inside-diameter test sections at flow rates ranging from $0.45 \times 10^4$ to $1.27 \times 10^4$ lb/(sq ft) (sec) (inlet velocities of 73 to 204 ft/sec). Results are presented for nonboiling forced convection, nucleate-boiling forced convection at local heat fluxes up to 11,200 Btu/(sq ft) (sec) ($40.3 \times 10^6$ Btu/(sq ft) (hr)), burnout, and pressure drop. All results are compared with existing correlations. The solution for the temperature distribution in a resistance-heated

Copies obtainable from NASA, Washington (over)

I. Schaefer, John W.
II. Jack, John R.
III. NASA TN D-1214

(Initial NASA distribution:
20, Fluid mechanics;
37, Propulsion system elements.)

NASA

NASA TN D-1214
National Aeronautics and Space Administration.
INVESTIGATION OF FORCED-CONVECTION NUCLEATE BOILING OF WATER FOR NOZZLE COOLING AT VERY HIGH HEAT FLUXES. John W. Schaefer and John R. Jack. May 1962. 46p. OTS price, $1.25. (NASA TECHNICAL NOTE D-1214)

The nonuniform axial heat-flux distribution typical of a very high temperature flow nozzle was simulated by resistance heating of variable-wall-thickness Inconel tubes. The coolant water flowed through the constant-inside-diameter test sections at flow rates ranging from $0.45 \times 10^4$ to $1.27 \times 10^4$ lb/(sq ft) (sec) (inlet velocities of 73 to 204 ft/sec). Results are presented for nonboiling forced convection, nucleate-boiling forced convection at local heat fluxes up to 11,200 Btu/(sq ft) (sec) ($40.3 \times 10^6$ Btu/(sq ft) (hr)), burnout, and pressure drop. All results are compared with existing correlations. The solution for the temperature distribution in a resistance-heated

Copies obtainable from NASA, Washington (over)

I. Schaefer, John W.
II. Jack, John R.
III. NASA TN D-1214

(Initial NASA distribution:
20, Fluid mechanics;
37, Propulsion system elements.)

NASA

NASA TN D-1214
National Aeronautics and Space Administration.
INVESTIGATION OF FORCED-CONVECTION NUCLEATE BOILING OF WATER FOR NOZZLE COOLING AT VERY HIGH HEAT FLUXES. John W. Schaefer and John R. Jack. May 1962. 46p. OTS price, $1.25. (NASA TECHNICAL NOTE D-1214)

The nonuniform axial heat-flux distribution typical of a very high temperature flow nozzle was simulated by resistance heating of variable-wall-thickness Inconel tubes. The coolant water flowed through the constant-inside-diameter test sections at flow rates ranging from $0.45 \times 10^4$ to $1.27 \times 10^4$ lb/(sq ft) (sec) (inlet velocities of 73 to 204 ft/sec). Results are presented for nonboiling forced convection, nucleate-boiling forced convection at local heat fluxes up to 11,200 Btu/(sq ft) (sec) ($40.3 \times 10^6$ Btu/(sq ft) (hr)), burnout, and pressure drop. All results are compared with existing correlations. The solution for the temperature distribution in a resistance-heated

Copies obtainable from NASA, Washington (over)

I. Schaefer, John W.
II. Jack, John R.
III. NASA TN D-1214

(Initial NASA distribution:
20, Fluid mechanics;
37, Propulsion system elements.)

NASA

NASA TN D-1214
National Aeronautics and Space Administration.
INVESTIGATION OF FORCED-CONVECTION NUCLEATE BOILING OF WATER FOR NOZZLE COOLING AT VERY HIGH HEAT FLUXES. John W. Schaefer and John R. Jack. May 1962. 46p. OTS price, $1.25. (NASA TECHNICAL NOTE D-1214)

The nonuniform axial heat-flux distribution typical of a very high temperature flow nozzle was simulated by resistance heating of variable-wall-thickness Inconel tubes. The coolant water flowed through the constant-inside-diameter test sections at flow rates ranging from $0.45 \times 10^4$ to $1.27 \times 10^4$ lb/(sq ft) (sec) (inlet velocities of 73 to 204 ft/sec). Results are presented for nonboiling forced convection, nucleate-boiling forced convection at local heat fluxes up to 11,200 Btu/(sq ft) (sec) ($40.3 \times 10^6$ Btu/(sq ft) (hr)), burnout, and pressure drop. All results are compared with existing correlations. The solution for the temperature distribution in a resistance-heated

Copies obtainable from NASA, Washington (over)

I. Schaefer, John W.
II. Jack, John R.
III. NASA TN D-1214

(Initial NASA distribution:
20, Fluid mechanics;
37, Propulsion system elements.)

NASA

NASA TN D-1214

variable-wall-thickness tube and the appropriate heat-transfer relations are derived.

Copies obtainable from NASA, Washington

NASA

NASA TN D-1214
National Aeronautics and Space Administration.
INVESTIGATION OF FORCED-CONVECTION NUCLEATE BOILING OF WATER FOR NOZZLE COOLING AT VERY HIGH HEAT FLUXES. John W. Schaefer and John R. Jack. May 1962. 46p. OTS price, $1.25. (NASA TECHNICAL NOTE D-1214)

The nonuniform axial heat-flux distribution typical of a very high temperature flow nozzle was simulated by resistance heating of variable-wall-thickness Inconel tubes. The coolant water flowed through the constant-inside-diameter test sections at flow rates ranging from $0.45 \times 10^4$ to $1.27 \times 10^4$ lb/(sq ft) (sec) (inlet velocities of 73 to 204 ft/sec). Results are presented for nonboiling forced convection, nucleate-boiling forced convection at local heat fluxes up to 11,200 Btu/(sq ft) (sec) ($40.3 \times 10^6$ Btu/(sq ft) (hr)), burnout, and pressure drop. All results are compared with existing correlations. The solution for the temperature distribution in a resistance-heated

Copies obtainable from NASA, Washington (over)

I. Schaefer, John W.
II. Jack, John R.
III. NASA TN D-1214

(Initial NASA distribution:
20, Fluid mechanics;
37, Propulsion system elements.)

NASA

NASA TN D-1214
National Aeronautics and Space Administration.
INVESTIGATION OF FORCED-CONVECTION NUCLEATE BOILING OF WATER FOR NOZZLE COOLING AT VERY HIGH HEAT FLUXES. John W. Schaefer and John R. Jack. May 1962. 46p. OTS price, $1.25. (NASA TECHNICAL NOTE D-1214)

The nonuniform axial heat-flux distribution typical of a very high temperature flow nozzle was simulated by resistance heating of variable-wall-thickness Inconel tubes. The coolant water flowed through the constant-inside-diameter test sections at flow rates ranging from $0.45 \times 10^4$ to $1.27 \times 10^4$ lb/(sq ft) (sec) (inlet velocities of 73 to 204 ft/sec). Results are presented for nonboiling forced convection, nucleate-boiling forced convection at local heat fluxes up to 11,200 Btu/(sq ft) (sec) ($40.3 \times 10^6$ Btu/(sq ft) (hr)), burnout, and pressure drop. All results are compared with existing correlations. The solution for the temperature distribution in a resistance-heated

Copies obtainable from NASA, Washington (over)

I. Schaefer, John W.
II. Jack, John R.
III. NASA TN D-1214

(Initial NASA distribution:
20, Fluid mechanics;
37, Propulsion system elements.)

NASA

NASA TN D-1214
National Aeronautics and Space Administration.
INVESTIGATION OF FORCED-CONVECTION NUCLEATE BOILING OF WATER FOR NOZZLE COOLING AT VERY HIGH HEAT FLUXES. John W. Schaefer and John R. Jack. May 1962. 46p. OTS price, $1.25. (NASA TECHNICAL NOTE D-1214)

The nonuniform axial heat-flux distribution typical of a very high temperature flow nozzle was simulated by resistance heating of variable-wall-thickness Inconel tubes. The coolant water flowed through the constant-inside-diameter test sections at flow rates ranging from $0.45 \times 10^4$ to $1.27 \times 10^4$ lb/(sq ft) (sec) (inlet velocities of 73 to 204 ft/sec). Results are presented for nonboiling forced convection, nucleate-boiling forced convection at local heat fluxes up to 11,200 Btu/(sq ft) (sec) ($40.3 \times 10^6$ Btu/(sq ft) (hr)), burnout, and pressure drop. All results are compared with existing correlations. The solution for the temperature distribution in a resistance-heated

Copies obtainable from NASA, Washington (over)

I. Schaefer, John W.
II. Jack, John R.
III. NASA TN D-1214

(Initial NASA distribution:
20, Fluid mechanics;
37, Propulsion system elements.)

NASA

NASA TN D-1214
National Aeronautics and Space Administration.
INVESTIGATION OF FORCED-CONVECTION NUCLEATE BOILING OF WATER FOR NOZZLE COOLING AT VERY HIGH HEAT FLUXES. John W. Schaefer and John R. Jack. May 1962. 46p. OTS price, $1.25. (NASA TECHNICAL NOTE D-1214)

The nonuniform axial heat-flux distribution typical of a very high temperature flow nozzle was simulated by resistance heating of variable-wall-thickness Inconel tubes. The coolant water flowed through the constant-inside-diameter test sections at flow rates ranging from $0.45 \times 10^4$ to $1.27 \times 10^4$ lb/(sq ft) (sec) (inlet velocities of 73 to 204 ft/sec). Results are presented for nonboiling forced convection, nucleate-boiling forced convection at local heat fluxes up to 11,200 Btu/(sq ft) (sec) ($40.3 \times 10^6$ Btu/(sq ft) (hr)), burnout, and pressure drop. All results are compared with existing correlations. The solution for the temperature distribution in a resistance-heated

Copies obtainable from NASA, Washington (over)

I. Schaefer, John W.
II. Jack, John R.
III. NASA TN D-1214

(Initial NASA distribution:
20, Fluid mechanics;
37, Propulsion system elements.)

NASA

NASA TN D-1214

variable-wall-thickness tube and the appropriate heat-transfer relations are derived.

Copies obtainable from NASA, Washington

NASA